

Catalytic Applications of Carbon Dots

Zhenhui Kang and Yang Liu

Abstract Carbon materials have been used for a long time in heterogeneous catalysis, which can satisfy most of the desirable properties required for a suitable catalyst support. Based on their significant advantages, such as low cost, huge amount, easy accessibility, high surface area, diverse porous structure, and resistance to acidic or basic environments, the carbon nanostructures are hungered for using as proper catalysts directly. Carbon dots (CDs), a new class of carbon nanomaterials with sizes below 10 nm, were also demonstrated to be efficient catalysts, such as, photocatalysts for selective oxidation, light-driven acid-catalysis and hydrogen bond catalysis. In this chapter, we will highlight the preparative methods, which have been used successfully to produce active, selective and durable CDs catalysts and look at their properties and the reactions which they promote. We then consider the catalysts design based on these new CDs and look into the future.

1 Preparative Methods

Here we just simple summarize the typical synthesis methods, and will not give a very detailed discussion. The detailed describe about the synthesis of CDs can be found in the recent reviews [1–5].

Tremendous efforts have been made to develop the synthetic methods for CDs. The methods have been proposed during the last decade can be roughly classified into “Top-down” and “Bottom-up” approaches. The top-down routes are implemented via either physical or chemical techniques, among which the latter is in the

Z. Kang (✉) · Y. Liu

Jiangsu Key Laboratory for Carbon-Based Functional Materials & Devices,
Institute of Functional Nano & Soft Materials (FUNSOM), Soochow University,
199 Ren'ai Road, Suzhou 215123, Jiangsu, China
e-mail: zhkang@suda.edu.cn

Y. Liu

e-mail: yangl@suda.edu.cn

majority. Further, the mechanism of chemical type top-down routes can be described as defect-mediated fragmentation processes. Namely, the oxygen-containing functional groups (epoxy and hydroxyl groups) could create defects on graphite sheets and serve as chemically reactive sites, thus allowing graphite to be cleaved into smaller sheets. Typically, the top-down methods include electron beam lithography, Laser ablation, acidic exfoliation, electrochemical oxidation, microwave-assisted hydrothermal synthesis, and so on. The top-down routes for the preparation of CDs have the advantages of abundant raw materials, large scale production and simple operation. CDs can also be prepared through bottom-up routes, including the solution chemistry, cyclodehydrogenation of polyphenylene precursors, carbonizing some special organic precursors or, the fragmentation of suitable precursors, for example, the C60. Compared with the up-down routes, the reports concerning the bottom-up routes are relatively scarce. The bottom-up methods offers us exciting opportunities to control the CDs with well-defined molecular size, shape, and thus properties. Nevertheless, these methods always involve complex synthetic procedures, and the special organic precursors may be difficult to obtain. Anyway, three problems facing CDs fabrication need to be noticed: (i) carbonaceous aggregation during carbonization, which can be avoided by using electrochemical synthesis, confined pyrolysis or solution chemistry methods, (ii) size control and uniformity, which is important for uniform properties and mechanistic study, and can be optimized via post-treatment, such as gel electrophoresis, centrifugation, and dialysis and (iii) surface properties that are critical for solubility and selected applications, which can be tuned during preparation or post-treatment. For particular applications explore, it is important to control the sizes of CDs to get uniform properties. Many approaches have been proposed to obtain uniform CDs during preparation or post-treatment. In most of the reports, the as-synthesized CDs fragments were purified via post treatments like filtration, dialysis, centrifugation, column chromatography and gel-electrophoresis. Surface modification is a powerful method to tune the surface properties of materials for selected applications. There are many approaches for functionalizing the surface of CDs through the surface chemistry or interactions, such as covalent bonding, coordination, p-p interactions, and sol-gel technology. Doping is a widely used approach to tune the PL properties of photoluminescent (PL) materials. Various doping methods with dozens of elements such as N, S, and P have been reported to tune the properties of CDs.

2 Structures and Properties of CDs

Here we just simple summarize the typical structure and properties of CDs, and will not give a very detailed discussion. The detailed describe about the structure and properties of CDs can be found in the recent reviews [1–5].

2.1 Component and Structure

In general, the average sizes of CDs are mostly below 10 nm, which is usually depended on the preparation methods. Technically speaking, CDs are only composed of elemental C and H. However, limit by their strong tendency for aggregation due to the face-to-face attraction and the preparation methods such as oxidation derived exfoliation, CDs reported so far are always partially oxidized, with hydroxyl, epoxy/ether, carbonyl and carboxylic acid groups on the surfaces. Fourier transform infrared (FTIR) and X-ray photoelectron spectroscopy (XPS) spectra are commonly adopted to analyze their component. The crystalline nature of CDs can be investigated through X-ray diffraction (XRD) patterns, Raman spectroscopy and high resolution transmission electron microscopy (HRTEM) observations. Both (002) interlayer spacing and (100) in-plane lattice spacing exist in CDs, and the former has been widely studied. The interlayer spacing of CDs depends strongly on their oxidation degree, that is, the attached hydroxyl, epoxy/ether, carbonyl and carboxylic acid groups can increase the interlayer spacing of CDs. The Raman technique is also a powerful and non-destructive tool for the characterization of CDs. The G band is assigned to the E_{2g} vibrational modes of the aromatic domains, whereas the D band arises from the breathing modes of the graphitic domains. Traditionally, the intensity ratio of “disorder” D to crystalline G (I_D/I_G) is used to compare the structural order between crystalline and amorphous graphitic systems. The I_D/I_G values of CDs vary significantly depending on the preparation methods. The HRTEM images of CDs features two kinds of lattice fringes, namely (002) interlayer spacing and (110) in-plane lattice spacing. Similar to the XRD pattern, the former centered at about 0.34 nm has been observed from CDs prepared by acidic oxidation from carbon black, microwave-assisted method, and electrochemical cutting method. The in-plane lattice spacing mostly centered at about 0.24 nm has been observed from CDS synthesized via microwave-hydrothermal protocol, amino-hydrothermal method, K intercalation, acidic oxidation from carbon fibers, and photo-Fenton reaction, excepting that valued at about 0.21 nm via hydrothermal cutting strategy and glucose carbonization method. Besides, these two kinds of lattice fringes have been simultaneously been observed in the case of electrochemical method from MWCNTs and acidic oxidation from natural graphite. Moreover, CDs are not always crystalline, amorphous CDs has also been prepared via hydrothermal method and citric acid carbonization.

2.2 Properties

Absorption. CDs typically show strong optical absorption in the UV region, with a tail extending out into the visible range. There may be some absorption shoulders attributed to the π - π^* transition of the C=C bonds, the n - π^* transition of C=O

bonds and/or others. Moreover, CDs prepared via different methods also showed different absorption behaviors. For instance, the citric acid carbonized CDs had an absorption band of 362 nm, but the unsubstituted HBC derived CDs with size of about 60 nm only showed a weak shoulder at 280 nm. Thus the absorption peak position was also dependent on the preparation method. Besides, the variation of oxygen content was reported to play important role in deciding the absorption peak position of CDs.

Photoluminescence. For both CDs, one of the most fascinating features is their photo-luminescence. Till now, variously sized CDs with different PL colors, ranging from the visible into the near-infrared region, have been prepared via various synthetic approaches. CDs prepared via different approaches can emit PL with different colors, including DUV, blue, green, yellow, and red. Typically, the luminescence mechanism may derive from intrinsic state emission and defect state emission. However, the exact mechanism of PL for CDs remains unsettled. The luminescence has been tentatively suggested to arise from excitons of carbon, emissive traps, quantum confinement effect, aromatic structures, oxygen-containing groups, free zigzag sites and edge defects. A widely accepted mechanism for luminescence emission from CDs needs systematic investigation. Anyway, the PL of CDs is should be attributed to either combining effect or competition between intrinsic state emission and defect state emission. CDs prepared via various methods probably exhibit distinct PL mechanism, which leads to different dependences of their PL on size, excitation wavelength, pH, solvent, and concentration etc. The quantum yield (QY) of CDs varies with the fabrication method and the surface chemistry involved. As for the unpassivated CDs, their QYs ranged between 2 and 30 %, which are observed in CDs prepared via stepwise solution chemistry and microwave-assisted acidic oxidation, respectively. The CDs commonly contains carboxylic and epoxide groups, which can act as the non-radiative electron-hole recombination centers. Therefore, the removal of these oxygen-containing groups maybe improves the QY, either by reduction or surface passivation. More importantly, significantly enhanced QY of ~ 72 % is the highest value for CDs reported so far [6].

Photoinduced electron transfer property. For the utilization of PL compounds in light-energy conversion and related areas, there have been extensive investigations on their photoresponse, photoinduced charge separation and electron transfer processes. It was found that the PL from a CDs solution could be efficiently quenched in the presence of either electron acceptors such as 4-nitrotoluene and 2,4-dinitrotoluene or electron donors such as N,N-diethylaniline. Namely, the photoexcited CDs are excellent as both electron donors and electron acceptors. They also found efficient PL quenching in CDs by surface-doped metals through disrupting the excited state redox processes. Electron transfer in nanocomposites of CDs-GO (graphene oxide), CDs-MWNTs (multi-wall carbon nanotubes) and CDs-TiO₂ NPs without linker molecules was also studied. Significant PL quenching was observed in the CD-GO system, which was attributed to the ultrafast electron transfer from CDs to GO with a time constant of 400 fs. In comparison, addition of carbon nanotubes resulted in static quenching of fluorescence in CDs. No charge

transfer was observed in either CD–MWNT or CD–TiO₂ nanocomposites. These interesting photoinduced electron transfer properties of CDs as an electron donor/acceptor may offer new opportunities for light energy conversion, catalysis and related applications, as well as mechanistic elucidation.

Bandgap engineering. CDs feature tunable bandgap due to their pronounced quantum confinement and edge effects. The bandgap in graphene-based materials can be tuned from 0 eV to that of benzene by changing size and/or surface chemistry, making it a rising carbon-based fluorescent material. Li et al. reported that the band gaps and redox potentials of CDs could be independently controlled, the former by size and the latter by functionalization. Based on the two major strategies, currently, increasing efforts have been made to customize their optical properties, among which the tunability based on the variation of size has already been discussed in the above section, Size dependence. Other strategies can be classified into three main groups: tuning oxidation degree, surface functionalization, and chemical doping, showing as below. The oxygen-containing functional groups on CDs can lead to radiative recombination of localized electron–hole pairs and surface emissive traps. And the variation of the degree of oxidation (or reduction) can induce the alteration of localized sp² clusters and structural defects, thus changing the PL. Chemical modifications using molecules with strong electron-donating or—accepting ability could also result in appreciable impact on electronic characteristics of grapheme. The electron-donating groups generally raised the HOMO levels, and electron-withdrawing groups lowered the LUMO levels. Doping carbon nanomaterials with heteroatoms can effectively tune their intrinsic properties, including electronic properties, surface and local chemical reactivity. In view of the remarkable quantum-confinement and edge effects of CDs, doping CDs with chemically bonded N atoms could drastically alter their electronic characteristics and offer more active sites, thus producing new phenomena and unique properties.

3 Catalytic Properties of CDs

3.1 Photocatalytic Activity for Selective Oxidation Reaction [7]

Selective oxidation of alcohols to carbonyls is a fundamental and significant transformation for the large-scale production of fine chemicals [8, 9]. Several UV and visible light driven photocatalytic systems for alcohols oxidation have been developed, such as Ru-(bipy)₃²⁺ and its derivatives, TiO₂ or TiO₂-based materials (dye/TiO₂), Pd@CeO₂, and mesoporous carbon nitride (mpg-C₃N₄) [9–18]. The photocatalytic application of carbon based materials has focused primarily on that such catalyst could or not catalyze the reaction by UV and/or visible light [19–22]. In general, the UV and/or short wavelength visible light may damage or change the

structure of organics [11–13]. From a broader perspective, exploiting long wavelength light driven photocatalysts is a direct and effective strategy to realize the photo-assisted selective organic transformations with high conversion and selectivity. 1–4 nm CDs are effective NIR light driven photocatalysts, which catalyze the efficient oxidation of benzyl alcohol to benzaldehyde with high conversion (92 %) and selectivity (100 %) in the presence of H₂O₂ as oxidant. The cooperation of CDs and NIR can prevent the overoxidation of the product to benzoic acid, and hold the reaction resting on the phase of benzaldehyde. Control catalytic experiments confirm that the catalytic activity of CDs is dependent on their photocatalytic activity for H₂O₂ decomposition and NIR light induced electron transfer property. Such metal-free photocatalytic system also selectively converts other alcohol substrates to their corresponding aldehydes with high conversion, demonstrating a potential pathway of accessing traditional alcohols oxidation chemistry. Details of the conversion and selectivity of benzyl alcohol oxidation catalyzed by CDs and contrast samples are shown in Table 1. After 12 h reaction under NIR light irradiation, high conversion efficiency of 92 % and high selectivity up to 100 % catalyzed by CDs (1–4 nm) were achieved simultaneously (Entry 1, Table 1). In contrast, CNPs (100–150 nm) and graphite (100–2000 nm) catalysts gave conversion of 71, 51 % and selectivity of only 78, 59 % under the same conditions, respectively (Entries 3 and 5). In the absence of NIR light, the selectivity yielded by three different catalysts all exhibited obvious decrease (Entries 2, 4 and 6), which means that the NIR light

Table 1 Selective oxidation of benzyl alcohol to benzaldehyde under the different light irradiation or not

Entry	Catalysts	Size (nm)	NIR light	Conv. (%) ^a	Sel. (%)
1	CDs	1–4	+	92	100
2	CDs	1–4	/ ^b	93	54
3	CNPs	100–150	+	71	78
4	CNPs	100–150	/	64	57
5	Graphite	100–2000	+	51	59
6	Graphite	100–2000	/	46	60
7 ^c	/	/	+	21	52
8	CDs	1–4	Vis ^d	93	84
9	CDs	1–4	UV ^e	95	75

All reactions were carried out applying a quartz three-neck flask. Typically, benzyl alcohol, CDs or other kinds of catalysts were added into a three-neck flask equipped with a condenser. The reaction mixture was vigorously stirred at 60 °C, followed by NIR irradiation for 12 h (450 W Xe arc lamp with an NIR-CUT filter to cut off light of wavelength <700 nm, remove the light when used control samples). H₂O₂ (30 wt% in water, 1.0 mL, 10.0 mmol) was added continuously with a syringe pump in 12 h

^aConversion rates were determined by GC with an FID detector

^bReference experiment without NIR light

^cReference experiment without catalyst

^dReference experiments with visible light

^eReference experiments with UV light

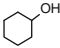
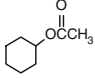
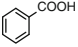
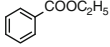
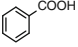
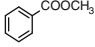

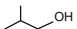
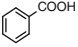
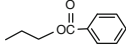
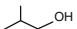
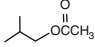
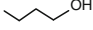
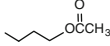
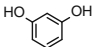
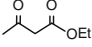
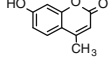
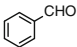
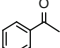
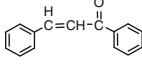
can enhance the catalytic ability of CDs for the selective oxidation. Here, the low selectivity yielded by contrast samples (Entries 2–6) are resulted from the formation of benzoic acid (overoxidation product of benzaldehyde) in the obtained products as measured by Gas Chromatography (GC) analysis. Additionally, in the absence of any catalyst, a thermocatalytic reaction of benzyl alcohol was observed for the same reaction system with low conversion (21 %) and poor selectivity (52 %) to benzaldehyde (Entry 8). When using CDs as catalyst and visible or UV light as the irradiation light (Entries 8 and 9), the conversion of benzyl alcohol (≤ 95 %) was similar to that using NIR light, while the selectivity to benzaldehyde (84, 75 %) was lower than that achieved under NIR light (100 %). These results reveal that the conversion and selectivity of such catalytic reaction are influenced not only by the carbon catalysts (CDs, CNPs, and graphite) but also by irradiation lights (UV, Vis, and NIR). The cooperation of CDs and NIR irradiation can promote the oxidation of benzyl alcohol to benzaldehyde achieving a high conversion and selectivity. Compared to the other catalysts with high efficiency (such as TiO_2 with a conversion and selectivity ca. 99 % under UV and visible light) [16], the catalytic process obtained the similar conversion (92 %) and selectivity (100 %) under long wavelength NIR light. Although the oxidants are different in these two systems, the long wavelength near infrared (NIR) and infrared (IR) light are more moderate and environmentally friendly than the UV light. The active oxygen species in the present process appear to have a radical character. The further experiments also strongly suggest that a higher amount of HO^\cdot would be generated by the unirradiated sample than that of the irradiated one. Without NIR irradiation, the mainly catalytic product is benzoic acid with only a little amount of benzaldehyde, indicating that during the reaction, benzyl alcohol is firstly oxidized into benzaldehyde, and then further oxidized into benzoic acid. Significantly, under the NIR light irradiation, the CDs' photo-induced electron transfer ability (especially as strong electron donors) protects the first step product (benzaldehyde) from overoxidation by the photoelectron reductive environment [23], thus yielding the high selectivity (100 %) to benzaldehyde. The scope of reactivity of the aforementioned CDs catalyst was further explored by Kang et al. using a variety of benzyl alcohol's derivatives under the same conditions under NIR light irradiations. Those benzyl alcohol's derivatives could also result into their oxidized aldehydes products in high conversions and selectivities with H_2O_2 as oxidant and NIR light irradiation.

3.2 Visible Light Induced Acid Catalyst [24]

The traditional acid catalysts (mineral acids, etc.) suffer from serious drawbacks that they necessitate costly and inefficient separation of catalysts from homogeneous reaction mixtures, resulting in a huge waste of energy and products, equipment corrosion, uncontrolled reaction, and demanding manufacturing conditions [25–33]. The use of solid acid catalysts offers advantages over liquid acids, such as reduced equipment corrosion, ease of product separation and catalyst recyclability [28–33].

Light-driven catalytic reactions can potentially provide a sustainable pathway for green controlled synthesis, and have attracted tremendous interest [34–37]. Carbon-based nanomaterials show great potential in photo-catalysis, redox-catalysis and acid-catalysis. As acid catalysts, carbon nanostructures (such as sulfated-graphene/-tube/-active carbons) typically suffer from lack of proper surface functionalization, low efficiency, and uncontrolled process [37–39]. 5–10 nm CDs have strong photo-induced proton generating capacity in solution under visible light irradiation. The catalytic activity of 5–10 nm CDs is strongly dependent on illumination intensity and reaction temperature. As light-driven acid-catalyst, they show CDs can catalyze a series of organic reactions (Esterification, Beckmann rearrangement and Aldol condensation) achieving high conversion efficiency in water solution under visible light irradiation. 5–10 nm CDs were produced from a graphite rod by electrochemical method in pure water. The reversible temperature- and concentration-dependent photo-proton generating ability should be due to the light-induced structure interconversion of the functional groups on CDs surface. And the proton generation mechanism of CDs under visible light irradiation was shown as follows. First, the hydroxyl group of CDs dissolved in water would release a free proton (or H_3O^+) under visible light irradiation. Then the intermediate would produce another proton (hydrolyzed to H_3O^+) from reaction of $\text{C}=\text{O}$ group with H_3O^+ . After the O in $\text{C}=\text{O}$ links with HO^- by supramolecular interaction, the intermediate with the epoxy group was obtained under visible light irradiation. A series of reactions (Esterification, Beckmann rearrangement, Aldol condensation) needing acid as a catalyst was performed by Kang et al. to study the photo-induced proton generating property of CDs and reference samples (small-sized CDs with 1–4 nm, graphite particles) [40]. The reaction products were monitored by GC. Details of different reactions (Esterification, Beckmann rearrangement, Aldol condensation) catalyzed by CDs and reference samples (Entry 1–10). After 10 h reaction under visible light irradiation, high conversion efficiencies of 34.7–46.2 % were achieved in all reactions (Esterification reactions: Entry 1–8; Beckmann rearrangement: Entry 9; Aldol condensation: Entry 10, Table 2) catalyzed by CDs. Under the same conditions but without visible light the, conversion efficiencies are substantially smaller at <5 % (Table 2), showing visible light can enhance the catalytic ability of CDs for acid-catalyzed reactions. To further investigate the role of light in the reaction, Kang et al. also measured conversion efficiency versus reaction time (Esterification, Beckmann rearrangement, and Aldol condensation corresponding to Entry 1, 9, and 10, respectively, were selected for study) in alternating dark and light environment. While, the conversion efficiencies of all three reactions increase sharply (4.1–6.8 %) under light irradiation (time at 0–30 min, 60–90 min, 120–150 min, and 180–210 min), but only a little (only 0.2–0.6 %) without irradiation. It shows that light irradiation indeed has an important effect on the acid catalytic reactions. In the absence of catalysts, a thermocatalytic reaction with a low conversion efficiency of <1 % was only observed in the reaction system. Moreover, the filtrate solution test, i.e. 2 h reaction after removing the CDs from the reaction medium, showed no catalytic activity. All above-mentioned experiments collectively show that CDs indeed can act as a light-controlled acid catalyst in the present catalytic reactions.

Table 2 Photocatalytic activities for different reactions (Esterification, Beckmann and Aldol condensation) by 5–10 nm CDs photocatalyst with (+) or without (–) light ($\lambda > 420$ nm) irradiation

Entry	Reactants 1	Reactants 2	Products	Conv. [%] (light +/-) ^a
1	CH ₃ OH	CH ₃ COOH	CH ₃ COOCH ₃	45.3/4.8
2		CH ₃ COOH		42.6/4.5
3	C ₂ H ₅ OH	CH ₃ COOH	CH ₃ COOC ₂ H ₅	43.7/4.2
4	C ₂ H ₅ OH			40.3/4.1
5	CH ₃ OH			38.9/3.7
6	 			45.2/4.3
7		CH ₃ COOH		39.1/4.0
8		CH ₃ COOH		35.5/3.9
9				46.2/4.5
10				34.7/3.8

All reactions were performed in a quartz three-neck flask. Reactants and CDs were added into a three-neck flask equipped with a condenser. The reaction mixture was vigorously stirred at low temperatures, followed by visible light irradiation for 10 h (450 W Xe arc lamp with a CUT filter to cut off light of wavelength <420 nm, but removed for experiments without irradiation)

^aConversion efficiencies were determined by GC with an FID detector

The catalytic activities of CDs in aqueous solution are attributed to the remarkable visible light-induced proton generating capability associated with the oxygen-containing functional groups of CDs.

3.3 Photoenhanced Hydrogen-Bond Catalytic Activity [41]

Hydrogen bonding (H-bonding) plays a crucial role in enzyme-catalyzed reactions by orienting the substrate molecules and lowering barriers to reactions [42]. Recently, this kind of noncovalent interaction (H-bonding) was introduced into

many organic chemical reactions [43–50], including the Diels-Alder, Aldol reaction, aza-Henry, Mannich, Michael, Morita-Baylis-Hillman, and Strecker reactions [51–58]. As a typical organocatalysis, hydrogen bond (H-bond) catalysis uses H-bonding interactions to accelerate organic reactions and stabilize anionic intermediates and transition states [59]. Several organic molecules with hydroxyl groups can be used as homogeneous H-bond catalysts [60–62]. For example, Chiral BINOL-derived Brønsted acids catalyze the enantioselective, asymmetric Morita-Baylis-Hillman (MBH) reaction of cyclohexenone with aldehydes [63]. Inorganic solid nanoparticles with abundant surface hydroxyl groups have been developed as alternative heterogeneous catalysts for H-bonding reactions [64, 65]. For example, aldol reactions could be catalyzed by hydroxyl groups on the $\text{Fe}(\text{OH})_3$ shell of $\text{Fe}_3\text{O}_4@ \text{Fe}(\text{OH})_3$ core-shell microspheres [66]. CDs are stable and biocompatible and have strong and tunable PL. CDs are considered to be good H-bonding catalysts because of their rich photochemical properties and functional carboxylic and hydroxyl groups. As heterogeneous nanocatalysts for H-bond catalysis, CDs showed good photoenhanced catalytic abilities (89 % yield when 4-cyanobenzaldehyde is used) in the aldol condensation. A series of catalytic experiments confirmed that the catalytic activity of CDs can be effectively enhanced by visible light, which may be attributed to their photo-induced electron accepting properties. The aldol condensation with a high yield of the aldol condensation product under CDs as catalyst. Typically, acetone was the solvent and reactant in the first set of trials and reacted with a series of aromatic aldehydes at room temperature. Detailed yields of the aromatic compounds are displayed in Table 3. As shown in Entry 8, the aldol condensation exhibited a very low yield in the absence of CDs as catalysts whether under light irradiation or not, confirming the CDs as catalyst is necessary for the reaction. In general, these reactions yielded higher yields with visible light irradiation than those produced in the dark. These data confirm that visible light is necessary for good conversion. When benzaldehyde (Entry 1) is used, the lowest yield in visible light (19 %) with CDs as catalyst (Table 3) was obtained. Other aromatic aldehydes (Table 3, Entries 2–7) showed higher conversion. Among them, when 4-cyanobenzaldehyde (circled by the red frame) is used, the aldol condensation showed the highest yield (89 %, Entry 5) with CDs as catalyst. These catalytic results were similar to the results reported by Niu et al. [66] It would be attributed to the weak interaction between the para-position of aldehyde group may have with and the groups on the CDs surface, which make the reactant molecules closer to the catalytic active center. In contrast, without visible light irradiation, yields were reduced to 18 % for 4-cyanobenzaldehyde (Entry 5). When the reaction temperature was elevated to 50 °C, a total conversion of 4-cyanobenzaldehyde in aldol condensation was achieved in 4 h (Table 3, Entry 9). When 4-chlorobenzaldehyde (Entry 2) and 4-bromobenzaldehyde (Entry 3) were used, the yields reached 68 and 63 %, respectively, with visible light irradiation, whereas the yields fell to 15 and 13 % in the dark. In the present system, the reaction products were dehydrated products, and the typical one (Table 3, Entry 1) was (E)-4-phenylbut-3-en-2-one. Different solvents (Toluene, Ethanol, THF, and CHCl_3) and ketones (cyclopentanone, cyclohexanone, and acetone) were selected to evaluate the catalytic abilities of CDs (about

Table 3 Room-temperature aldol condensation between acetone and aromatic aldehydes in the presence of CDs with or without visible light

Entry ^a	Ar-	Light ^b	Dark ^c
		Yields (%) ^d	Yields (%)
1	C ₆ H ₅	19	3
2	4-Cl-C ₆ H ₄	68	15
3	4-Br-C ₆ H ₄	63	13
4	4-NO ₂ -C ₆ H ₄	65	8
5	4-CN-C ₆ H ₄	89	18
6	4-CH ₃ -C ₆ H ₄	67	9
7	4-CH ₃ O-C ₆ H ₄	65	8
8 ^e	4-CN-C ₆ H ₄	Trace	Trace
9 ^f	4-CN-C ₆ H ₄	99	32

^aReaction conditions: 0.2 mmol aromatic aldehydes, 2 mL acetone, 60 mg CDs, room temperature, 24 h

^{b,c}Reference experiments with and without visible light irradiation, respectively (Xenon lamp, 300 W, $\lambda \geq 420$ nm)

^dThe reaction products were isolated through silica column chromatography, and analyzed by GC

^eReference experiment without catalyst

^fHeated to 50 °C, 4 h

5 nm) for aldol condensations with 4-cyanobenzaldehyde. When ethanol, THF, and CHCl₃ were used as solvents, the highest yield when 4-cyanobenzaldehyde is used (32 %) was obtained with THF as solvent. The lowest yield (12 %) was for CHCl₃. In the catalytic system, toluene was the most suitable solvent for the aldol condensation with CDs as catalysts. CDs with three different average particle sizes (5, >10, and <4 nm) were tested. The highest yield of 89 % was achieved for 5 nm CDs when 4-cyanobenzaldehyde is used, whereas yields of 40 and 25 % were obtained for CDs >10 and <4 nm, respectively. 5 nm CDs had the most satisfying photocatalytic performance for this H-bond catalysis reaction, which should attribute to the highest electron accepting ability when compared with other CDs (with size >10 and <4 nm). Further, control catalytic experiments confirmed that the efficient electron-accepting properties of CDs strengthened the O–H bond and activated the C=O bond of the 4-cyanobenzaldehyde, accelerating the aldol condensation.

3.4 Visible-Light Photocatalysts for CO₂ Conversion [67]

The significant rise in atmospheric CO₂ levels due to the combustion of hydrocarbon fuels has generated much concern. Among various CO₂ sequestration options, a compelling approach is photocatalytic conversion to recycle CO₂ back to hydrocarbon fuels, for which the use of solar irradiation may represent an ultimate solution. However, there are major challenges in finding potent photocatalysts

[68, 69]. Nanoscale wide-band-gap semiconductors such as titanium dioxide (TiO_2) and cadmium sulfide (CdS) were originally used and have since been quite popular in CO_2 photoreduction and related photocatalytic reactions, but their limitations in terms of the requirement for UV excitation and generally low conversion efficiencies have also become evident [68–70]. The functionalized carbon nanoparticles with gold or platinum coating were used as photocatalysts for the reduction of CO_2 . In a typical experiment, an aqueous solution of the goldcoated particles was added to an optical cell in the photolysis setup, after which the solution was purged with CO_2 gas toward saturation at ambient temperature. The resulting solution in the optical cell was photoirradiated with visible light for 5 h. The photoreduction of CO_2 generally yields formic acid as a significant product. The quantification of the photoproduct was used to estimate quantum yields for photocatalytic reactions of CO_2 under the specific experimental conditions [71]. For the reduction to formic acid only, the estimated quantum yield was $\sim 0.3\%$, which was likely lower than the overall quantum yield for the CO_2 conversion. Nevertheless, even for the production of formic acid alone, the observed quantum yield is already at the higher end of the available literature values for reactions with a variety of photocatalysts under many different conditions. As a more direct comparison, the use of suspended TiO_2 nanoparticles (Degussa P25) as photocatalysts with UV light irradiation (through a 350 nm cutoff filter) in the same photolysis setup resulted in quantum yields that were an order of magnitude lower (also for formic acid only). For the platinum-coated photocatalysts in the CO_2 conversion reaction under otherwise identical experimental conditions, the results were generally similar to those with the gold-coated ones described above, though more quantitative comparisons, including those for effects of varying amounts of metal coating, are still being pursued. Mechanistically, photoexcitation of the surface-passivated small carbon nanoparticles likely results in charge separation to form surface-confined electrons and holes, on which significant experimental evidence has already become available [72, 73]. For example, the bright fluorescence emissions, which can be attributed to radiative recombinations on the particle surface, could be quenched by both electron donors and acceptors in an equally efficient fashion [72]. The emissions were also essentially diminished by the gold or platinum coating, as the coated metal was designed to soak up the surface-confined electrons, disrupting the radiative recombinations. Therefore, the functionalized carbon nanoparticles apparently served the function of harvesting visible photons to drive the photoreduction process, with the particle surface defects facilitating the charge separation by trapping the separated electrons and holes, phenomenologically similar to what occurs for metal-coated semiconductor nanoparticles (e.g., platinum-coated CdS or TiO_2) [74–76]. In addition to the obviously important advantage of strong visible absorption, other distinctive features of the nanoscale carbon-based photocatalysts include their aqueous solubility for the photoconversion under homogeneous reaction conditions and the confinement of the photoinduced charge separation to the particle surface, thus facilitating more efficient electron harvesting by the coated gold or platinum as the cocatalyst in the CO_2 conversion. Beyond CO_2 photoreduction, the same functionalized carbon nanoparticles with gold or platinum coating

could be used as photocatalysts for H_2 generation from water [77, 78]. In present system, the photoconversion efficiencies likely benefit from the solubility of the catalysts, surface confinement of the photoinduced charge separation and trapping, and the straightforward doping of metal cocatalysts.

3.5 Photocatalyst for Overall Water-Splitting [79]

Electronic structural analysis revealed that graphene oxide (GO) materials have conduction band minimum (CBM) and valence band maximum (VBM) levels suitable for generating H_2 and O_2 , respectively, under visible-light irradiation [80]. Size modulation and chemical modification readily tune the electronic properties of graphene. The size effect results from quantum confinement, which becomes prominent when the sp^2 domain size is less than 10 nm. Quantum confinement causes the separation of the π and π^* orbitals, and creates a band gap in graphene [81–86]. Modifying graphene by oxygen adsorption forms C–O covalent bonds that damage the original orbitals and confine π electrons because of the reduction in sp^2 domain size. This modification renders the quantized discrete levels to be dictated by the nature of the sp^2 domains and associated functional groups. GO is a p-doped material because oxygen atoms are more electronegative than carbon atoms. Replacing oxygen functional groups on the GO sheet edge with nitrogen-containing groups transforms GO into an n-type semiconductor. In addition to surface modification by addition of functionalities, direct substitution with heteroatoms in the graphene lattice induces the modulation of optical and electronic properties. Teng et al. synthesized nitrogen-doped grapheme oxide-quantum dots (NGO-QDs) as the catalyst [79]. The NGO-QDs exhibited both p- and n-type conductivities. The diode configuration resulted in an internal Z-scheme charge transfer for effective reaction at the QD interface. Visible light (>420 nm) irradiation on the NGO-QDs resulted in simultaneous H_2 and O_2 evolution from pure water at an $H_2:O_2$ molar ratio of 2:1. An energetic band bending was present at the interface between semiconductor and solution, and a p–n type photochemical diode configuration, mimicking the biological photosynthesis system, provided a favorable situation to accomplish vectorial charge displacement for overall water-splitting. These developed NGO-QD photocatalyst consisted of nitrogen-doped graphene sheets stacked into crystals, with oxygen functional groups on the crystal surface. The band gap of the NGO-QDs was approximately 2.2 eV, and was capable of absorbing visible light to generate excitons. This NGO-QD construction resulted in the formation of p–n type photochemical diodes, in which the n-conductivity was caused by embedding nitrogen atoms in the graphene frame, and the p-conductivity by grafting oxygen functionalities on the graphene surface. Visible-light illumination on NGO-QDs suspended in pure water resulted in the evolution of H_2 and O_2 at a molar ratio of approximately 2:1. The p- and n-domains were responsible for the production of H_2 and O_2 gases, respectively. Nitrogen-free QDs with p-type conductivity catalyzed only H_2 evolution under irradiation, proving that the band bending in the p-type

domains was favorable for electron injection to produce H_2 . Likewise, NH_3 -treated NGO-QDs showed n-type conductivity and catalyzed only O_2 evolution. The sp^2 clusters serve as the junction between the p- and n-domains and are the recombination sites for majority carriers from the two domains. The strong PL emission from the NGO-QDs with visible-light irradiation might be associated with the presence of the interfacial junction for recombination. The photochemical diode-type mechanism for water-splitting over NGO-QDs showed a remarkable similarity to that of biological photosynthesis [79].

3.6 CDs as Electrocatalysts [5]

Nitrogen doping has been a powerful way to modify the properties of carbon materials. N-doping was also demonstrated to significantly affect the properties of the CDs, including the emergence of size-dependent electrocatalytic activity for the oxygen reduction reaction. For technological relevance in clear energy production like fuel cells and clear fuel production, oxygen reduction reaction (ORR) and its reverse reaction—oxygen evolution reaction (OER) are at the centre of intensive research. Because of the sluggish kinetics of ORR, electrocatalysts are usually used to improve the kinetics of ORR and of which platinum is the “state-of-the-art”. Unfortunately, the formidably high cost of platinum-based electrocatalysts has prompted researchers to look for non-platinum-based electrocatalysts for ORR, aiming at achieving comparable or even better electrocatalytic efficiency than that of platinum-based electrocatalysts. The ultra-small size of CDs along with their high stability and good electrical conductivity makes them interesting contenders as electrocatalytic materials for ORR [87]. Previous investigations on graphene have indicated that doped nitrogen atoms in carbon materials, especially in the form of pyridinium moieties, play a critical role in enhancing their electrocatalytic activities toward ORR. One of the pioneering reports on the use of CDs as electrocatalysts for ORR was by Li et al. [88]. They demonstrated that N-CDs with oxygen-rich functional groups prepared via an electrochemical procedure are electrocatalytically active toward electrochemical reduction of oxygen. The onset potential of ORR was found to be -0.16 V (vs. Ag/AgCl), which is close to that of commercial platinum-based electrocatalysts. Similar results were later obtained by Yan and co-workers and Liu et al. With N-CDs synthesised by totally different procedures [89, 90]. A comparison between nitrogen-free CDs and the N-CDs suggested that the electrocatalytic activity of the N-CDs is indeed closely associated with the N-doping effect. In addition, the N-CDs exhibited excellent tolerance to a possible crossover effect from methanol. First-principles investigations of the N-CDs suggested that pyridinic and graphitic nitrogen are responsible for the observed electrocatalytic activity [91]. In another report, Zhu and colleagues investigated the electrocatalytic activity of CDs prepared from natural biomass—soy milk [92].

Similar to the N-CDs, a much enhanced electrochemical reduction profile of oxygen was obtained. Likewise, OER also suffers from sluggish kinetics and a high over-potential is required in order to drive OER at a reasonably high rate. Currently, the best electrocatalysts for OER are ruthenium- and iridium-based materials. Again, the formidably high cost of these materials has urged researchers to search for alternative electrocatalysts that can offer high efficiency in OER and yet readily available at low cost. Unfortunately, reasonably high electrocatalytic activity of CDs toward OER has yet to be reported.

4 Catalysts Design Based on Carbon Dots

4.1 From CDs to Mesoporous Carbons Catalyst [93]

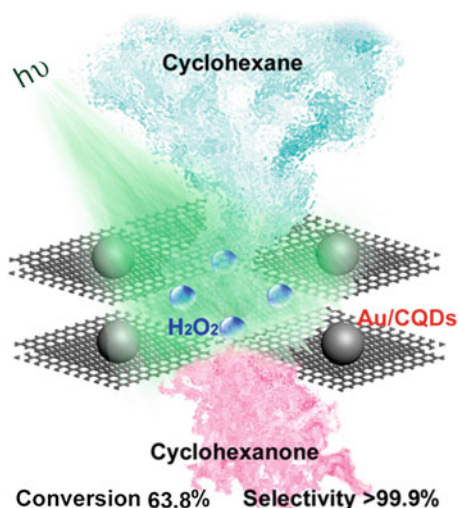
The design, fabrication and control of nanostructured materials are the core issues in catalysis and nanotechnology [94–96]. Carbon nanostructures, as typical inorganic materials, such as carbon nanotube, graphene, mesoporous carbon, have received a great deal of attention due to its wide applications [97–100]. Especially, mesoporous carbons (MCs) are widely used for gas separation, adsorbents, catalyst supports, and electrodes for electrochemical double layer capacitors and fuel cells [101–108]. Although many kinds of rigid and designed inorganic templates have been employed to obtain MCs with uniform pore sizes, the synthesis process still suffers from complex steps, harsh conditions, and a series post-processing [109, 110]. Therefore, seeking a facile and non-template method to obtain MCs is still a huge challenge for nanochemistry and nanotechnology. In light of their tiny size, high crystalline nature (fragments of graphite) and functionalized surface, CDs should be regarded as the construction units of carbon materials, and then realize the construction of mesoporous carbon without templates. The obtain MCs from CDs have a high specific surface area ($183.6 \text{ m}^2 \text{ g}^{-1}$) and uniform pore size distribution (5 nm). Typically, during the synthetic process of MCs, firstly, with the temperature increased, the water molecule would lose by β -elimination/condensation reactions from the hydroxyl/carboxyl groups on the surface of CDs, which makes the graphitic structure developed as well as the formation of carbon–oxygen-carbon bonds. After the further dehydration and/or carbonization, many CDs were connected with each other and finally lead to the formation of MCs. Also, MCs as catalyst exhibit high catalytic activity for selective oxidation of cyclooctene (32.43 % conversion based on cyclooctene and 87.53 % selectivity for epoxycyclooctane) with tert-Butyl hydroperoxide (TBHP) as initiator and air as oxidant at 80 °C. The high conversion of cyclooctene and selectivity to epoxycyclooctane was achieved simultaneously after 48 h. The conversion efficiency of cyclooctene increased from 7.81 to 32.43 % after 48 h. The selectivity of epoxycyclooctane also increased from 75.53 up to 87.53 %. But the selectivity to 2-cyclooctenone fell to 9.23 from 24.47 % with increasing reaction time. MCs catalyst really have good catalytic activity over the

elective oxidation of cyclooctene. Moreover, the present selective oxidation of cyclooctene was carried out under a mild condition with air as oxidant, which suggested that the present process is energy-saving, environment-friendliness, and low cost. The oxygen-containing surface groups indeed are active sites for the elective oxidation of cyclooctene and have an effect on the catalytic activity of MCs.

4.2 *Metal Nanoparticle/CD Complex Photocatalyst for Hydrocarbon Selective Oxidation [111]*

The selective oxidation of cyclohexane to cyclohexanone and cyclohexanol (about 10^6 tons per year) is the key step of the commercial production of nylon-6 and nylon-66 polymers. Despite extensive development efforts for cyclohexane oxidation catalysts, today's commercial processes still suffer from high temperature (150–160 °C), high pressure (1–2 MPa), low yield (<15 %), low selectivity (<80 %), and excessive production of wastes [112, 113]. Catalysts enabling cyclohexane oxidation under mild conditions would alleviate the potential hazard of harsh reaction conditions, as well as allow for more selective and controlled reactions. As a preferred oxidant in liquid phase, hydrogen peroxide can work at low temperature, produces only water as a by-product and has a high oxygen uptake (47 %) [114–116]. However, cyclohexane oxidation with H_2O_2 at low temperature using the current catalysts (such as weak acid resin, iron bispidine complexes, Ru complex, Cr/Ti/Si oxides, Na-GeX, mesoporous TS-1, Ti-MCM-41, metal aluminophosphates, biomimetic systems and Cu–Cr₂O₃) invariably suffers from large amount of organic solvent (i.e. acetone and acetonitrile), poor selectivity, and low H_2O_2 efficiency, thus making its industrialization difficult [117–126]. CDs can function not only as an efficient photocatalyst (for highly selective oxidation), but also as a multi-functional component in photocatalyst design to promote wider spectrum absorption and separation of electron-hole, as well as to stabilize photolysis semiconductors [40]. Metal nanoparticles (Au, Cu, etc.) are known to possess catalytic activities for selective oxidation reactions [127, 128]. Additionally, surface plasma resonance absorption can also induce good photocatalytic abilities of metal nanoparticles (Au, Ag, etc.) [129, 130]. Kang et al. report the design of a tunable photocatalyst based on the composite of CDs and metal nanoparticles for the selective oxidation of cyclohexane. Significantly, the Au nanoparticles/CDs (Au/CDs) composite catalyst yielded oxidation of cyclohexane to cyclohexanone with 63.8 % efficiency and >99.9 % selectivity in the presence of H_2O_2 under visible light at room temperature (see Fig. 1). The totality of the experiments shows that the high conversion and selectivity in the present photocatalyst system should be attributed to the collective contribution and interactions of CDs and AuNPs. In present photocatalytic system, the reaction happened in the interface between Au NPs and CDs. Although the hydroxy radicals have strong oxidation abilities, the synergic effect of the functions of CDs and the SPR (surface

Fig. 1 Au/CQDs composites as a photocatalyst for selective oxidation of cyclohexane in the presence of H_2O_2 under visible light (reproduced from Liu et al. [111, p. 328])



plasmonic resonance) of AuNPs, still can protect the products (cyclohexanone and cyclohexanol) from the over oxidation. The totality of the experiment results suggests the following mechanistic processes in the photocatalytic oxidation of cyclohexane. The surface plasma resonance of AuNPs enhances the light absorption of Au/CDs composites. Under visible light, H_2O_2 is decomposed to hydroxyl radical (HO^\cdot), which serves as a strong oxidant for conversion of cyclohexane to cyclohexanone. In the process, the interaction between CDs and AuNPs under visible light plays a key role in the eventual high conversion and selectivity. Based on the proposed mechanism, Ag nanoparticles/CDs (Ag/CDs) and Cu nanoparticles/CDs (Cu/CDs) composite photocatalysts were synthesized, and used to catalyze cyclohexane oxidation under the same condition with Au/CDs system. Like the Au/CDs system, Ag/CDs and Cu/CDs composites exhibited similarly good catalytic performance under purple light (conversion 54.0 %, selectivity 84.1 % for Ag) and red light (conversion 46.7 %, selectivity 75.3 % for Cu), which correspond respectively to the surface plasma resonance of Ag and Cu nanoparticles. The results were consistent with the proposed catalytic mechanism discussed above. It is therefore possible to tune the wavelength response of the present photocatalyst system based on the surface plasma resonance of metal nanoparticles to achieve high-efficiency and high-selectivity oxidation of cyclohexane. Given its diversity and versatility of structural and composition design, metal nanoparticles/CDs composites may provide a powerful pathway for the development of high-performance catalysts and production processes for green chemical industry.

4.3 *CDs/Ag/Ag₃PW₁₂O₄₀ Photocatalysts for Overall Water Splitting [131]*

The traditional strategy for designing photocatalysts for overall water splitting is based on metal oxide systems with activities that are related to the band gap and photogenerated electron-hole pairs [132–138]. Typically, photocatalysts are divided into three groups according to the electronic configuration of their core metal ions. (1) Transition metal ions with d^0 configurations are Ti^{4+} , Zr^{4+} , Ta^{5+} , Nb^{5+} , V^{5+} , and W^{6+} . (2) A rare-earth metal ion with an f^0 configuration is Ce^{4+} . (3) Typical metal ions with d^{10} configurations are Ga^{3+} , In^{3+} , Ge^{4+} , Sn^{4+} , and Sb^{4+} [70, 139–146]. Unfortunately, the majority of the photocatalysts are complex and expensive or function only with ultraviolet (UV) irradiation in need of an appropriate electron acceptor or hole scavenger. Although some semiconductors, such as La-doped NaTaO_3 , Ni-doped InTaO_4 and $(\text{Ga}_{1-x}\text{Zn}_x)\text{-(N}_{1-x}\text{O}_x)$ solid solution (or to construct a Z-scheme structure), are employed to realize the overall water-splitting, these catalyst systems still suffer from the low light absorption (<510 nm), poor separation efficiency of electron-hole pairs, and the formidable complexity of the oxidative half-reaction [147–152]. Polyoxometalates (POMs), with unique photoelectric chemical properties, are potentially useful for photocatalytic H_2 and O_2 generation [153–158]. The utilization of surface plasmon resonance (SPR) has offered a new opportunity to overcome the limited efficiency of photocatalysts. SPR improves the solar-energy-conversion efficiency by (i) extending light absorption to longer wavelengths, (ii) increasing light scattering, and (iii) exciting electron-hole pairs in the semiconductor by transferring the plasmonic energy from the metal to the semiconductor [159]. In light of the remarkable photocatalytic properties of CDs, the SPR effect of metal Ag, and the photocatalytic hydrogen generation of POMs, the combination of CDs, Ag, and POMs may be a unique approach to construct stable and efficient complex photocatalyst for solar water splitting. Kang and Liu et al. report the design and fabrication of CDs/Ag/Ag₃PW₁₂O₄₀ nanocomposites, which served as photocatalysts for overall water splitting in visible light (light absorption extend to 650 nm) without any electron acceptors or hole scavengers. The estimated apparent quantum yield (AQY) was 4.9 % at 480 nm [143, 160]. A reaction mechanism was proposed to explain the photocatalytic water splitting with this composite photocatalyst in visible light. In present system, POMs play a key role for the water splitting. PB could be formed under visible light irradiation in a complex system [161, 162]. The absorption of visible light happened at Ag nanoparticles surface for the SPR effect, and then the absorbed photons would be efficiently separated into electrons and holes. Given the dipolar character of the surface plasmonic state of Ag nanoparticles, such those electrons made POM transfer to PB which resulted from the one- and two-electron reduced, and the holes will act as positive charge centers on the Ag₃PW₁₂O₄₀ surface [163, 164]. Also, PB could be further excited by visible light irradiation and transferred electrons to conductive band of POM as literatures reported [165–167]. These non-tight-binding electrons in the intermediate energy levels act like as “color center” in Ag₃PW₁₂O₄₀,

which can be transiently stabilized and further photoexcited to the conduction band of $\text{Ag}_3\text{PW}_{12}\text{O}_{40}$ by photons in visible regions. On the other hand, the photoexcited electrons in the conduction band of $\text{Ag}_3\text{PW}_{12}\text{O}_{40}$ are thermodynamically feasible for water reductions. The Ag nanoparticles here played two vital roles for the enhanced photocatalytic water splitting efficiency: (1) the strong SPR-induced electric fields localized nearby at the Ag/ $\text{Ag}_3\text{PW}_{12}\text{O}_{40}$ interfaces which can cause the electrons generation and enhance separation efficiencies of electron-hole pairs in $\text{Ag}_3\text{PW}_{12}\text{O}_{40}$ [168]; and (2) The electrons in the conduction band of $\text{Ag}_3\text{PW}_{12}\text{O}_{40}$ can inject into the contractile Ag nanoparticles which act as electron buffer and catalytic site for hydrogen generation. The insoluble CDs layer on the surface of $\text{Ag}_3\text{PW}_{12}\text{O}_{40}$ effectively protects $\text{Ag}_3\text{PW}_{12}\text{O}_{40}$ from dissolution in aqueous solution, thus, enhancing the structural stability of CDs/Ag/ $\text{Ag}_3\text{PW}_{12}\text{O}_{40}$ during the photocatalytic processes. Also, the CDs with excellent storing-charges ability can also act as like an electron buffer which can promote the electron-extraction from the conduction band of $\text{Ag}_3\text{PW}_{12}\text{O}_{40}$ and subsequently decrease the electron-hole recombination rate in $\text{Ag}_3\text{PW}_{12}\text{O}_{40}$ and increase the optical absorption of $\text{Ag}_3\text{PW}_{12}\text{O}_{40}$ for the increased unoccupied occupiable-states in the conduction band of $\text{Ag}_3\text{PW}_{12}\text{O}_{40}$ [168, 169]. Finally, CDs can enhance the electron transport due to their photo-induced electron transfer property. All of above mentioned positive roles of Ag, CDs, and $\text{Ag}_3\text{PW}_{12}\text{O}_{40}$ are responsible for the excellent photocatalytic water splitting properties of the composited CDs/Ag/ $\text{Ag}_3\text{PW}_{12}\text{O}_{40}$ photocatalysts in visible light.

4.4 CDs Sensitized TiO_2 Nanotube Arrays for Photoelectrochemical Hydrogen Generation Under Visible Light [170]

TiO_2 is regarded as one of the most popular photoanode materials of photoelectrochemical (PEC) water splitting devices owing to its high resistance to photo-corrosion, physical and chemical stability, easy availability and low cost. While, both the bulk and nanostructured photoanodes of pure TiO_2 materials still suffer the major limitation of weak response (or nonresponse) to the visible spectrum owing to their large band gap (about 3.2 eV). To date, a variety of strategies have been utilized to improve TiO_2 PEC performance, such as doping with C, N, Sn, Sr, Nb, coupling with secondary semiconductors and photosensitization of dyes [171–176]. Compared with the doping strategy, another approach with dye-based compounds or narrow band gap semiconductors as a sensitizer is convenient, and has structure and properties designable abilities [173–181]. This system also has achieved a certain degree of success in broadening the absorption spectrum to visible and near infrared (NIR) region, and therefore enhancing the solar-to-hydrogen (STH) efficiency of the PEC cells [174, 177–181]. For the efficient hydrogen generation under visible light, a good sensitizer should meet several criteria as described in the following. First, it

must be able to enhance the absorption of the solar spectrum for the host materials. Second, it should own suited energy levels so that the photoexcited electrons in the HOMO level or conduction band can be efficiently injected into the semiconductor acceptor's conduction band, and simultaneously the holes in the LUMO level or valence band can oxidize the reducing substances in the electrolytes. Third, it is favorable to contain some specific functional groups on their surfaces which can make them easy and stable to attach to the semiconductor acceptors' surfaces. Fourth, it should be resistant to corrosion or degradation in the practical operation conditions of PEC cells for a long term. CDs were used as an alternative sensitizer for the PEC cells based on TiO₂ nanotube arrays (TiO₂ NTs). Under simulated sunlight illumination (AM 1.5G, 100 mW/cm²), the photocurrent density of the CDs sensitized PEC cell is four times larger than the unsensitized one at 0 V versus Ag/AgCl. The corresponding hydrogen production rate was determined to be about 14.1 μmol/h for a CDs sensitized TiO₂ nanotube arrays (CDs/TiO₂ NTs) photoanode (about 0.78 cm²) with Faradaic efficiency nearly 100 %. The enhanced photocurrent after CDs deposited on the surface of TiO₂ is not due to the TiO₂ were excited by the CDs' upconverted emission. This conclusion was confirmed by the different IPCE results obtained by performing tests in different electrolytes. No positive IPCE value can be observed with excited wavelength over 410 nm for CDs/TiO₂ NTs photoelectrode in 1 M Na₂SO₄ aqueous electrolyte. The reason is that the holes in the HOMO level of CDs are not able to realize the oxygen evolution reaction (OER) while they can be consumed by the hole-scavenger in a sacrificial electrolyte such as Na₂S/Na₂SO₃ aqueous solution. And if the positive IPCE values over 410 nm observed by performing the measurement in the Na₂S/Na₂SO₃ aqueous solution were due to the upconverted fluorescence of CDs, there should also be able to observe a positive IPCE value over 410 nm in the 1 M Na₂SO₄ electrolyte. Therefore, a sensibilization mechanism was proposed to illustrate the role of CDs in the PEC cells. A photon with adequate energy can excite the electron in the HOMO level transferring to the LUMO level of CDs. Afterward, the excited electrons in the LUMO level of the CDs are transferred to the conduction band of the contacted TiO₂ NTs and then transported to the counter electrode for hydrogen evolution reaction along the TiO₂ NTs axial direction. While the holes left in the HOMO level of the CDs can oxidize the sacrificial reagent to complete a whole galvanic circle. It can be expected that several further works could be done to optimize the PEC hydrogen production efficiency of the CDs/TiO₂ system: (a) one can design more reasonable structures of TiO₂ to improve the absorbance of CDs and the charge carrier transport; (b) CDs can be modified by doping with S, N and P to further enhance the light-harvesting ability, quantum efficiency and the chemical reaction kinetics; (c) Surface treatments of CDs may be favorable for stronger anchoring on TiO₂ and higher photogenerated charge carrier separation efficiency.

4.5 *Modulation of Electron/Energy Transfer States at TiO₂-CDs Interface [182]*

In light of their respective unique properties, CDs and TiO₂ nanotubes (TNTs) arrays may be integrated into a model nanosystem for the studies of catalysis, photoelectrical devices, and energy transfer systems in chemistry and nanoscience. Different energy and electron transfer states have been observed in the CDs/TNTs system due to the up-conversion photoluminescence and the electron donation/acceptance properties of the CDs decorated on TNTs. Kang and wang et al. show a bias-mediated electron/energy transfer process at the CDs/TiO₂ interface for the dynamic modulation of opto-electronic properties [182]. Different energy and electron transfer states have been observed in the CDs/TNTs system due to the up-conversion PL and the electron donation/acceptance properties of the CDs layer. Specifically, five distinct electron/energy transfer states of the CDs-decorated TiO₂ nanotubes (CDs/TNTs) system can be dynamically tuned by different pulse-bias treatments. To investigate the photoelectrochemical and electron/energy transfer process in the CDs/TNTs system, a series of photoelectrochemical experiments was performed in a two-electrode cell system with Pt as the counter electrode. The mechanism of the present pulse-bias tunable opto-electronic conversion logic phenomenon in the CDs/TNTs system as follows. When the negative bias applied to the CDs/TNTs electrode was increased from -1 , -2 , to -3 V, the positively charged CDs would be attracted increasingly closer to TNTs, leading to gradual reduction in interface impedance. At 0 and -1 V pulse-bias treatment, or high and medium interface impedance, photo-excited electrons of TNTs would favor to transfer to the Pt electrode, and those of CDs would favor to return to a low-energy state. And then the up-converted PL of CDs would excite the TiO₂, leading to higher IPCE_{max} (opto-electronic conversion). At -2 V pulse-bias treatment, or low interface impedance, the symbiotic effect of up-converted PL of CDs and high electron transfer ability between TNTs and CDs would lead to the highest IPCE_{max} (opto-electronic conversion). While at -3 V pulse-bias treatment, the interface impedance between TNTs and CDs would be lowest, and recombination of photo-induced electrons and holes of TNTs through TiO₂-CDs-TiO₂ pathway be highest, thus leading to least up-converted PL and lowest opto-electronic conversion. The present pulse-bias treatment method would enable the opto-electronic conversion logic phenomenon in the CDs/TNTs nanosystem. Application of different pulse-bias treatment can generate high, medium or low opto-electronic conversion efficiency. The IPCE of electrode increased from 13.5 to 19 % after -1 V pulse-bias treatment, and from 13.5 to 24 % after -2 V pulse-bias treatment, but decreased from 13.5 to 2.5 % after -3 V pulse-bias treatment. This phenomenon represents a simple logic function, which yields a medium output at no bias (or low positive pulse bias), a high output at -2 V pulse bias, and a low output at -3 V pulse bias. Significantly, the programmable character (based on different applied bias potential) of the present system is extremely versatile and facile. This bias-mediated electron/energy transfer process at the

CDs/TiO₂ interface may provide a new opportunity not only for the manipulation of opto-electronic conversion process, but also for the development of opto-electronic conversion devices and photocatalyst design.

4.6 *CDs Stabilized Gold Nanoparticles Catalyst System [183]*

General speaking, the adsorption effect should be taken into the consideration firstly to improve the catalytic activity and stability, which is the precondition and crucial process in nanocatalyst design of catalytic reactions. Au nanoparticles (AuNPs), with their excellent electronic, magnetic, optical, thermal, catalytic, and biochemical properties, [184–187] have been intensively studied in many fields (such as sensors, biolabeling, drug delivery, and photonics), especially as novel catalysts for catalysis [185–192]. However, the catalytic chemistry of AuNPs still face some challenges, such as, the catalytic activity needs to be improved and AuNPs are still unstable in the reaction process. It was expected to enhance the adsorption capacity and stability of AuNPs based nanocatalysts to improve the catalytic efficiency. CDs with abundant functional groups (–OH, –COOH, C=O) in surface were especially designed to enhance the adsorption capacity and the catalytic activity of AuNPs. The CDs stabilized gold nanoparticles (AuNPs-CDs) were greenly synthesized by one-step reduction H₂AuCl₄ with CDs used as both reductant and stabilizer under visible light irradiation. The resulted AuNPs-CDs possess high catalytic activity toward 4-nitrophenol reduction. Further detailed adsorption kinetics data indicated that the present adsorption systems follow predominantly the second-order rate model and CDs capped on the surface of AuNPs also enhanced the adsorption capacity and the catalytic activity of AuNPs. CDs have been successfully used in photocatalyst design and optical sensor due to their excellent chemical and optical properties [193, 194]. From the view of catalyst design, the novel advantages of CDs used in catalysis are as follows: First, CDs have suited sizes (below 10 nm) for catalysis system [40]. Second, CDs have excellent photo-chemical properties (photoinduced electron transfer and redox properties, luminescence and so on) [195]. Third, the surface of CDs is adjustable with overall oxygen contents ranging from 5 to 50 wt%, depending upon the experimental conditions used [196]. Finally, the functional groups (–OH, –COOH, etc.) in surface of CDs are helpful for improving the adsorption of reactants [197–200]. Therefore, CDs are good candidates for nanocatalyst design. CDs were specially designed to enhance the adsorption capacity and catalysis activity of AuNPs. The abundant functional groups (–OH, –COOH, C=O) in the surface of CDs not only can reduce H₂AuCl₄ to AuNPs but also can enhance the stability of AuNPs in a water-based environment [201–204]. The resultant AuNPs-CDs show excellent hydrophilic, high stability and good bio-compatible. Adsorption kinetics manifests the present AuNPs-CDs sorption systems

follow predominantly the second-order rate model. The synthesized AuNPs-CDs also can be used as an efficient catalyst for toxic pollutant 4-NP totally reduction to 4-AP (conversion, 100 %). A good linear correlation of $\ln(C_t/C_0)$ versus time was obtained and a kinetic rate constant of AuNPs-CDs was determined to be 0.68 min^{-1} . The functional groups ($-\text{OH}$, $-\text{COOH}$, $-\text{C}=\text{O}$) in surface of CDs are good for enhancing the adsorption capacity and then the catalytic activity of AuNPs. In present system, the results obviously indicated CDs capped on the surface of AuNPs enhanced the adsorption and stability of AuNPs, which accorded with the highly catalytic activity of AuNPs-CDs. The equilibrium of sorption was evaluated by two well-known models of Langmuir and Freundlich isotherm. The Langmuir isotherm model is the most widely used two-parameter equation, which assumes monolayer adsorption onto a surface containing a limited number of adsorption sites with no transmigration of the adsorbate in the plane of the surface. The Freundlich isotherm in the other hand takes heterogeneous systems into account and is not restricted to the formation of the monolayer. The Langmuir isotherm with correlation coefficient of 0.995 and 0.997 represents a better fit of experimental data than Freundlich model with correlation coefficient of 0.982 and 0.975, for CDs and AuNPs-CDs, respectively. It indicates that monolayer adsorption of 4-NP takes place on the homogeneous surface of AuNPs-CDs adsorbents. Moreover, the adsorption is favorable and rather irreversible. Based on the results of adsorption and reduction rate, it suggests that CDs help in adsorbing 4-nitrophenol ions closer to the surface of AuNPs, AuNPs subsequently help in facilitating the reduction of 4-NP by lowering the activation energy of the reaction and play the role of catalyst. Adsorption kinetics manifests that the present AuNPs-CDs sorption systems follow predominantly the second-order rate model.

4.7 Photocatalyst Design Based on CDs and Semiconductor Nanoparticles [40, 168, 169]

CDs/TiO₂ Photocatalysts [40]. As one of the most popular photocatalysts, TiO₂ has been used in the removal of organic pollutants and in the generation of H₂ through water splitting. However, a major drawback in its photocatalytic efficiency resides in its ineffective utilisation of visible light as the irradiation source. Because the bandgap of bulk TiO₂ lies in the UV region (3.0–3.2 eV), only less than 5 % of sunlight is utilised by TiO₂. TiO₂-CD nanocomposites are able to completely degrade MB (50 mg mL⁻¹) within 25 min under visible light irradiation, where only <5 % of MB is degraded when pure TiO₂ is used as the photocatalyst. Apart from harvesting visible light and converting it to shorter wavelength light through up-conversion, which in turn excites TiO₂ to form electron-hole pairs, it is believed that the CDs in the nanocomposites facilitate the transfer of electrons from TiO₂ and the electrons can be shuttled freely along the conducting paths of the CDs, allowing charge separation, stabilisation and hindering recombination, thereby generating

long-lived holes on the TiO_2 surface. The longer-lived holes then account for the much enhanced photocatalytic activity of the TiO_2 -CD nanocomposites. Likewise, similar behavior was observed with SiO_2 -CD nanocomposites in the photocatalytic degradation of MB36 and selective hydrocarbon oxidation. Nonetheless, more work is needed to improve the lifespan of the above-mentioned photocatalysts before they can be employed in practical scenarios.

In addition to being used as photocatalysts, CDs have been capturing the attention of researchers as potential photosensitizers in solar cells [205]. For example, a CD-RhB- TiO_2 system showed that the CDs effectively bridge the RhB molecules to the TiO_2 substrate by acting as a one-way electron transfer intermediary. Comparing to the RhB- TiO_2 system, the presence of CDs significantly enhanced the photoelectric conversion efficiency by as much as seven times. In another report, a CD/ TiO_2 electrode was employed in a solar cell. The photocurrent density was 2.7 times larger than that of pristine TiO_2 electrode under visible light illumination. Enhanced performance of a solar cell was also obtained when N-CDs were used as photosensitizers. Although the photo-to-electricity conversion efficiency of the above-mentioned solar cells is far from satisfactory, these findings definitely encourage more research in the application of CDs in photovoltaic devices and photocatalyst design [205].

CDs/ Ag_3PO_4 Photocatalysts [168]. Ag_3PO_4 is slightly soluble in aqueous solution, which greatly reduces its structural stability. During the photocatalytic process, the transformation of Ag^+ into Ag is usually accompanied, which results in the photocorrosion of Ag_3PO_4 in the absence of electron acceptors. Furthermore, along with the photocatalytic reaction, the appearance of the by-products, black metallic Ag particles would inevitably prevent visible light absorption of Ag_3PO_4 , which decrease the photocatalytic activity. CDs display abundant photo-physical properties. Especially, the strong size and excitation wavelength dependent PL behaviors further enhance their photocatalytic properties. Considering such remarkable properties of CDs and the limitations of the Ag_3PO_4 photocatalytic system, the combination of CDs and Ag_3PO_4 may be regarded as an ideal strategy to construct the stable and efficient complex photocatalytic system (such as, CDs/ Ag_3PO_4 and CDs/Ag/ Ag_3PO_4 photocatalysts). The key roles of CDs in the complex photocatalysts were soundly investigated. The CDs layer on the surface of Ag_3PO_4 and Ag/ Ag_3PO_4 particles can effectively protect Ag_3PO_4 from dissolution in aqueous solution. The unique photoinduced electron transfer properties of CDs can make Ag_3PO_4 avoid photocorrosion. The up-converted PL property of CDs make the CDs/ Ag_3PO_4 and CDs/Ag/ Ag_3PO_4 complex systems effectively utilize the full spectrum of sunlight to greatly enhance the photocatalytic activity. Moreover, CDs can act as an electron reservoir to hinder the electron/hole pairs' recombination probability. More interestingly, the existence of Ag accompanied by SPR can further enhance the utilization of sunlight and formation of electron/hole

pairs. The synergistic effects of CDs and Ag lead to the highest photocatalytic activity of CDs/Ag/Ag₃PO₄ complex photocatalyst.

CDs/Cu₂O Photocatalysts [169]. So far, near infrared (NIR) and IR light (total called (N)IR) of sunlight (account for 53 %) are still not fully utilized by present photocatalytic system, which has become gradually an urgent challenge for chemistry and materials science. To effectively utilize the (N)IR light, an ideal photocatalytic system should be effectively activated by (N)IR light. As discussed above, the TiO₂/CDs and SiO₂/CDs complex systems were demonstrated to show excellent photocatalytic ability in visible light, while they are still impuissant in (N)IR wavelength zone. In light of its relative narrow band gap (about 2.2 eV), high photostability, and low toxicity, Cu₂O was a potential candidate for designing the CDs based (N)IR light sensitive photocatalyst. It was reported that the CDs/Cu₂O photocatalytic system could harness the (N)IR light to enhance the photocatalytic activity based on the collective effect of superior light reflecting ability of the Cu₂O protruding nanostructures and the up-converted PL property of CDs. When the CDs/Cu₂O composite photocatalyst is illuminated, the protruding nanostructures allow the multiple reflections of (N)IR light among the vacant space between these protruding particles, which can make better use of the source light and therefore offering an improved photocatalytic activity. On the other hand, CDs can absorb (N)IR light (>700 nm), and then emit shorter wavelength light (390–564 nm) as a result of up-conversion, which in turn further excites Cu₂O to form electron/hole (e⁻/h⁺) pairs. The electron/hole pairs then react with the adsorbed oxidants/reducers (usually O₂/OH⁻) to produce active oxygen radicals (e.g. ·O₂, ·OH), which subsequently cause the degradation of organic dye (MB). Significantly, when CDs are attached on the surface of Cu₂O, the relative position of CDs band edge permits the transfer of electrons from the Cu₂O surface, allowing the charge separation, stabilization, and then hindering e⁻/h⁺ pairs' recombination. The electrons can be shuttled freely along the conducting network of CDs, and the longer-lived holes on the Cu₂O then account for the higher activity of the composite photocatalyst. In addition, for organic pollution degradation, the p-p interaction between conjugated structure of CDs and benzene ring of MB is beneficial to the enrichment of MB on the surface of CDs/Cu₂O composite.

4.8 CDs/NiFe Layered Double Hydroxide Composite Electrocatalyst [206]

The oxygen evolution reaction (OER) is kinetically slow owing to its multistep proton-coupled electron transfer process, so the electrolysis must require a relative high potential than thermodynamic potential for water-splitting. 10 RuO₂ and IrO₂ are regarded as the most active OER catalysts, but the lacking of Ru and Ir makes it impractical to use the metals on a large scale [207–209]. Layered double hydroxides (LDHs), as a family of layered anionic materials, have attracted considerable

attention because of their flexible structures and chemical versatility, which have been exploited as a fruitful source of materials with applications in electrochemistry, magnetism, catalysis and chemical sensing [210–213]. NiFe-LDH possesses a layered and relatively open structure, which makes it much easier for rapid diffusion of reactants/products, and even fast proton-coupled electron transfer process in water oxidation reaction. But the poor electrical conductivity restricts its massive applications in electrocatalysis. Although other carbon-related materials (such as carbon nanotubes (CNTs), graphene) have been reported to composite with LDHs for electrocatalysis applications, their poor charge transport efficiencies and complicated functional groups design are still weaknesses [214–216]. While, CDs known as a novel class of nanocarbon with abundant functional groups on the surface which are needed for nucleating and anchoring the pristine nanocrystals with CDs solidly to achieve intense electrostatic interaction (or covalent attachment), have attracted considerable attention because of their unique physical or chemical properties. The CDs/NiFe-LDH complex exhibits high electrocatalytic activity (with overpotential ~ 235 mV in 1 M KOH at a current density of 10 mA cm^{-2}) and stability for oxygen evolution. This almost exceeded those of any previous Ni–Fe compounds and even was comparable to that of the lowest overpotential reported in Ni–Fe catalysts, ~ 230 mV at 10 mA cm^{-2} for electrodeposited Ni–Fe films [169, 207, 217]. Typically, nickel acetate and iron nitrate (with a molar ratio of Ni/Fe = 5) were hydrolyzed in a mixed N,N-dimethylformamide (DMF) and CDs aqueous solution at 85°C for 4 h. Followed by redispersing the intermediate product in a DMF/H₂O mixed solvent and through a solvothermal treatment at 120°C for 12 h, then a second solvothermal step at 160°C for 2 h. The solvothermal treatment may lead to the crystallization of NiFe-LDH nanoplates and formation of the nanocomposites. The high electrocatalytic property was primarily attributed to the NiFe-LDH phase, and further enhanced by strong associating the LDH with CDs, which possess small size, excellent conductivity, rapid electron transfer, and electron reservoir properties. Specifically, the small size of CDs may provide large specific surface area for more convenient electrocatalytic reaction. And the rapid electron transfers from CDs to NiFe-LDH on the surface could further improve the electrocatalytic activities. The surface functional groups on CDs (such as, carboxy C=O) make it easier for the formation of CDs/NiFe-LDH composites solidly due to the strong electrostatic interactions between NiFe-LDH and CDs (or generating new covalent bond (like C–O–Ni or C–O–Fe)). Anyway, through synergistic effect between NiFe-LDH and CDs afforded by direct integrating the Ni–Fe LDH nanoplates with the surface functional groups on CDs contributed to the optimal OER activity of the CDs/NiFe-LDH composite catalysts. Given the diversity and versatility of structural design of the present CDs/NiFe-LDH composite system, the combination of CDs and NiFe-LDH nanoplates as a superb electrocatalyst may provide a new approach to high-efficiency CDs-related electrocatalysts design for applications towards new energy sources, green chemistry, and environmental issues.

4.9 CDs for Porous Co, N-Codoped Carbon Electrocatalyst Design [218]

Although materials based on Pt are believed to be the most effective electrocatalysts for ORR, they still suffer from the high cost and poor supply of Pt, promoting the research on highly active catalysts [219–222]. Numerous studies have focused on the preparation of low-cost Co based nitrogen-containing materials as electrocatalysts for ORR, in which the heat-treatment of macrocyclic compounds under the inert atmosphere was found to be an effective method for the preparation of such Co/N/C catalysts [223–225]. For example, Chang et al. studied the effect of the structures of pyrolyzed cobalt-based macrocyclic compounds on ORR and proposed that the pyrolyzed cobalt-corrin compounds (py-Co-Corrin/C) exhibited the highest activity for ORR [226]. Zagal et al. [227] studied the application of Vitamin B12 (VB12) absorbed on graphite electrode for ORR. Liang et al. [228] investigated the mesoporous catalyst fabricated from VB12 and silica nanoparticles exhibited a remarkable activity for ORR in acid medium with half-wave potential of 0.79 V versus reversible hydrogen electrode (RHE). Wang et al. reported a series of applications of pyrolyzed VB12 as non-precious metal catalyst for ORR in polymer electrolyte fuel cells (PEFC) and microbial fuel cells (MFC) [229]. Although these Co, N-codoped materials were demonstrated to be potential non-precious catalysts for ORR, there are still underlying problems yet to be dealt with urgently: such as, the finely control and optimization of Co and N concentrations, which is closely related to the catalytic ability optimization; the construction of porous structure; whether the Co and N concentrations affect the electrocatalytic activity for ORR synergistically. The solutions of above issues are of great importance and will effectively promote widespread application of Co/N/C catalysts [218]. With the aim of constructing a material with large surface area and well crystalline structure in favor of electron transportation, CDs could be regarded as the promising building blocks as a result of their tiny size, highly crystalline structure (they are fragments of graphite) and functionalized surface. Taking advantages of CDs, the pyrolysis of VB12 and CDs could lead to the porous structure and well controlled concentrations of Co and N, which are beneficial for the enhancement of electrocatalytic activity of catalyst. In a typical experiments, CDs and VB12 were utilized as raw materials to fabricate Co/N/C catalysts [218]. The porous cobalt, nitrogen-codoped carbon materials (Co/N/C) were synthesized by a facile one-step pyrolysis of VB12 and CDs. Varying the initial mass ratio of CDs and VB12 leads to controllable concentrations of Co (0–3.88 %) and N (0–5.88 %) after pyrolysis. The obtained Co/N/C was evaluated by ORR in both alkaline and acid media. Particularly, the Co/N/C with 1.12 % Co and 2.92 % N prepared at 700 °C exhibited the best catalytic ability for ORR with cathodic peak at –0.165 and 0.185 V (vs. SCE) in 0.1 M KOH and 0.1 M HClO₄ solution, respectively, which are comparable to that of Pt/C (20 %). The obtain catalyst also showed long-term stability and high methanol tolerance, which outperforms commercial Pt/C (20 %). According to the rotating disk electrode (RDE) and rotating

ring-disk electrode (RRDE) results of Co_{1.12}/N_{2.92}/C-700 catalyst, the numbers of electron-transferred for the ORR were calculated to be 3.6, which indicated a four-electron pathway. Our results further demonstrated that the Co_{1.12}/N_{2.92}/C-700 catalyst showed superior methanol tolerance and durability than the commercial Pt/C (20 %) in alkaline and acid media. With the increase of Co concentration, the peak potential shifts to more positive and reach a maximum at the optimum Co concentration of 1.12 %, then shifts negatively. For the effect of N concentration on the ORR peak potential, the peak potential reaches a maximum at N concentration of 2.92 %. On the other hand, with the increase of Co doping concentration, the current density increases and reaches the maximum value of 1.16 mA cm⁻² at 1.12 % for Co then drops with the increase of Co concentration. While, the highest current density is obtained when the doping concentration of N is 2.92 %. More or less N concentration will lead to the decrease of the current density. Co/N/C with 1.12 % Co and 2.92 % N exhibits the highest current density in acid medium. These results indicate that the Co and N concentrations exhibit a synergistic effect on the catalytic ability of Co/N/C system. Although, at present stage, no more information was provided to confirm the most optimized Co, N doping concentrations for ORR catalytic ability of Co/N/C system, the present results still demonstrate a primary rule for electrocatalyst design and component contents optimization to achieve more efficient catalyst: The effects of Co and N doping concentrations on the catalytic ability of Co/N/C are synergistic. With the increase of Co and N concentrations, the catalytic ability of Co/N/C increases to reach a maximum at the concentration of 1.12 % for Co and 2.92 % for N, respectively, then decreases with higher doping concentration of Co and N (Co > 1.12 and N > 2.92). The stability of Co_{1.12}/N_{2.92}/C-700 was investigated by chronoamperometric measurements in O₂ saturated 0.1 M KOH and 0.1 M HClO₄ solution. The continuous oxygen reduction reaction causes only a slight loss (7 %) of the current for Co_{1.12}/N_{2.92}/C-700 catalyst after 4000s of reaction under alkaline condition. As a comparison, the current loss on Pt/C (20 %) is as high as 26 % after the same reaction duration. The excellent ability of Co_{1.12}/N_{2.92}/C-700 was attributed to the existence of clusters with excellent crystallinity and porous structure which resulted in formation of large interface and surface. These factors facilitated the transportation of electrons. The numbers of electron-transferred for the ORR were calculated to be around 3.6, which indicated the four-electron pathway.

5 Outlook [1–5]

In this chapter, we have described the recent advances in the research on C-dots, focusing on their synthesis, properties, and applications in catalysis. The examples given above are taken from the literature published until December 2014. We believe that many other reactions will be studied using CDs nanocatalysts and some of them will undoubtedly give new examples of catalysis by CDs.

A variety of synthesis techniques already exist for producing CDs of different characteristics. The PL and optical properties of C-dots are both interesting and intriguing, constituting a rich and hot research topic. The general strategy for the adoption of environmentally benign CDs as photocatalysts in synthetic chemistry represents an attractive approach in the development of green chemistry, which may eventually lessen the burden of energy consumption, product clean-up and waste disposal. The immediate goal in this emerging area should be geared toward the discovery of photochemical solutions for increasingly ambitious synthetic goals. The long-term goals should be to improve efficiency and synthetic utility and to eventually perform chemical synthesis under sunlight. Compared to other applications of CDs, there have been fewer studies in the usability of CDs as electrocatalysts for ORR and OER. In-depth theoretical and experimental studies are needed to delicately design CD-based electrocatalysts with desirable electrocatalytic activity and long-term operation stability. The combination of CD doping and CD-based nanocomposites with other nanomaterials may open up new avenues to systematically study the effect of structural parameters and chemical compositions on the catalytic performance of the electrocatalysts, thus leading to fundamental insights and practical applications. The potential of CDs in the storage and transport of electrons impacted by light has yet to be exploited fully.

In the future, we expect the advent of more facile and robust synthetic routes and creative applications to better realize the potential of the increasingly important CDs materials. New properties and how to subtly tune these properties, such as fresh phosphorescence and debatable up-converted PL, are also challengeable for its nubilous luminescent mechanism. The amorphous to nearly crystalline internal structure, nonquantitative surface structure and virtual size polydispersion may block the clarification of the luminescence mechanism. This problem will be solved through the accurate synthesis, careful analysis, and intelligent consideration. CDs stand to have a huge impact in biotechnological and environmental applications because of their potential as nontoxic alternates to traditional heavy-metal-based QDs. In addition, the unique photoinduced electron transfer ability, as well as excellent light harvesting capability, make CDs an exceptional candidate for photocatalytic and photovoltaic applications. Carefully designed C-dots composites have the potential to expand the capabilities of next-generation energy-storage and photovoltaic devices, photocatalysts and sensors. By surface and band gap modification of CDs via functionalization or semiconductors, we can expect to design novel catalysts from CDs for green chemistry and energy issues.

References

1. S.N. Baker, G.A. Baker, Luminescent carbon nanodots: emergent nanolights. *Angew. Chem. Int. Ed.* **49**, 6726–6744 (2010). doi:[10.1002/anie.200906623](https://doi.org/10.1002/anie.200906623)
2. H. Li, Z. Kang, Y. Liu, S.T. Lee, Carbon nanodots: synthesis, properties and applications. *J. Mater. Chem.* **22**, 24230 (2012). doi:[10.1039/C2JM34690G](https://doi.org/10.1039/C2JM34690G)

3. L.L. Li, G.H. Wu, G.H. Yang, J. Peng, J.W. Zhao, J.J. Zhu, Focusing on luminescent graphene quantum dots: current status and future perspectives. *Nanoscale* **5**, 4015 (2013). doi:[10.1039/C3NR33849E](https://doi.org/10.1039/C3NR33849E)
4. Y.F. Wang, A.G. Hu, Carbon quantum dots: synthesis, properties and applications. *J. Mater. Chem. C* **2**, 6921 (2014). doi:[10.1039/C4TC00988F](https://doi.org/10.1039/C4TC00988F)
5. S.Y. Lim, W. Shen, Z.Q. Gao, Carbon quantum dots and their applications. *Chem. Soc. Rev.* **44**, 362 (2015). doi:[10.1039/C4CS00269E](https://doi.org/10.1039/C4CS00269E)
6. J. Sun, S. Yang, Z. Wang, H. Shen, T. Xu, L. Sun, H. Li, W. Chen, X. Jiang, G. Ding, Z. Kang, X. Xie, M. Jiang, Ultra-high quantum yield of graphene quantum dots: aromatic-nitrogen doping and photoluminescence mechanism. *Part. Part. Syst. Charact.* (2014). doi:[10.1002/ppsc.201400189](https://doi.org/10.1002/ppsc.201400189)
7. H. Li, R. Liu, S. Lian, Y. Liu, H. Huang, Z. Kang, Near-infrared light controlled photocatalytic activity of carbon quantum dots for highly selective oxidation reaction. *Nanoscale* **5**, 3289–3297 (2013). doi:[10.1039/C3NR00092C](https://doi.org/10.1039/C3NR00092C)
8. G. Palmisano, E. Garcia-Lopez, G. Marci, V. Loddo, S. Yurdakal, V. Augugliaro, L. Palmisano, Advances in selective conversions by heterogeneous photocatalysis. *Chem. Commun.* **46**, 7074 (2010). doi:[10.1039/C0CC02087G](https://doi.org/10.1039/C0CC02087G)
9. M. Zhang, Q. Wang, C. Chen, L. Zang, W. Ma, J. Zhao, Oxygen atom transfer in the photocatalytic oxidation of alcohols by TiO₂: oxygen isotope studies. *Angew. Chem. Int. Ed.* **48**, 6081 (2009). doi:[10.1002/anie.200900322](https://doi.org/10.1002/anie.200900322)
10. K. Kalyanasundaram, Photophysics, photochemistry and solar energy conversion with tris (bipyridyl)ruthenium(II) and its analogues. *Coord. Chem. Rev.* **46**, 159–244 (1982). doi:[10.1016/0010-8545\(82\)85003-0](https://doi.org/10.1016/0010-8545(82)85003-0)
11. B. Liu, F. Wu, N.-S. Deng, UV-light induced photodegradation of 17 α -ethynylestradiol in aqueous solutions. *J. Hazard. Mater.* **98**, 311 (2003). doi:[10.1016/S0304-3894\(02\)00321-7](https://doi.org/10.1016/S0304-3894(02)00321-7)
12. Y. Zhang, J.L. Zhou, B. Ning, Photodegradation of estrone and 17 β -estradiol in water. *Water Res.* **41**, 19 (2007). doi:[10.1061/j.watres.2006.09.020](https://doi.org/10.1061/j.watres.2006.09.020)
13. A.S. Kumar, T. Ye, T. Takami, B.-C. Yu, A.K. Flatt, J.M. Tour, P.S. Weiss, Reversible photo-switching of single azobenzene molecules in controlled nanoscale environments. *Nano Lett.* **8**, 1644 (2008). doi:[10.1021/nl1080323+](https://doi.org/10.1021/nl1080323+)
14. M. Zhang, C.C. Chen, W.H. Ma, J.C. Zhao, Visible-Light-induced aerobic oxidation of alcohols in a coupled photocatalytic system of dye-sensitized TiO₂ and TEMPO. *Angew. Chem. Int. Ed.* **47**, 9730 (2008). doi:[10.1002/ange.200803630](https://doi.org/10.1002/ange.200803630)
15. N. Zhang, S.Q. Liu, X.Z. Fu, Y.-J. Xu, A simple strategy for fabrication of “Plum-Pudding” Type Pd@CeO₂ semiconductor nanocomposite as a visible-light-driven photocatalyst for selective oxidation. *J. Phys. Chem. C* **115**, 22901–22909 (2011). doi:[10.1021/jp205821b](https://doi.org/10.1021/jp205821b)
16. S. Higashimoto, N. Kitao, N. Yoshida, T. Sakura, M. Azuma, H. Ohue, Y. Sakata, Selective photocatalytic oxidation of benzyl alcohol and its derivatives into corresponding aldehydes by molecular oxygen on titanium dioxide under visible light irradiation. *J. Catal.* **266**, 279–285 (2009). doi:[10.1016/j.jcat.2009.06.018](https://doi.org/10.1016/j.jcat.2009.06.018)
17. Q. Wang, M. Zhang, C.C. Chen, W.H. Ma, J.C. Zhao, Photocatalytic aerobic oxidation of alcohols on TiO₂: the acceleration effect of a Brønsted acid. *Angew. Chem. Int. Ed.* **49**, 7976 (2010). doi:[10.1002/anie.201001533](https://doi.org/10.1002/anie.201001533)
18. Z.-R. Tang, Y.H. Zhang, Y.-J. Xu, Tuning the optical property and photocatalytic performance of titanate nanotube toward selective oxidation of alcohols under ambient conditions. *ACS Appl. Mater. Interfaces*, **4**, 1512 (2012). doi:[10.1021/am3001852](https://doi.org/10.1021/am3001852)
19. Z.H. Kang, E.B. Wang, B.D. Mao, Z.M. Su, L. Gao, L. Niu, H.Y. Shan, L. Xu, Heterogeneous hydroxylation catalyzed by multi-walled carbon nanotubes at low temperature. *Appl. Catal. A* **299**, 212 (2006). doi:[10.1016/j.apcata.2005.10.038](https://doi.org/10.1016/j.apcata.2005.10.038)
20. D.R. Dreyer, H.-P. Jia, C.W. Bielawski, Graphene oxide: a convenient carbocatalyst for facilitating oxidation and hydration reactions. *Angew. Chem. Int. Ed.* **49**, 6813 (2010). doi:[10.1002/ange.201002160](https://doi.org/10.1002/ange.201002160)

21. J. Zhang, X. Liu, R. Blume, A. Zhang, R. Schlogl, D.S. Su, Surface-modified carbon nanotubes catalyze oxidative dehydrogenation of n-butane. *Science* **322**, 73–77 (2008). doi:[10.1126/science.1161916](https://doi.org/10.1126/science.1161916)
22. J. Pyun, Graphene oxide as catalyst: application of carbon materials beyond nanotechnology. *Angew. Chem. Int. Ed.* **50**, 46 (2011). doi:[10.1002/anie.201003897](https://doi.org/10.1002/anie.201003897)
23. Z.H. Kang, C.H.A. Tsang, N.-B. Wong, Z.D. Zhang, S.T. Lee, Silicon quantum dots: a general photocatalyst for reduction, decomposition, and selective oxidation reactions. *J. Am. Chem. Soc.* **129**, 12090 (2007). doi:[10.1021/ja075184x](https://doi.org/10.1021/ja075184x)
24. H. Li, R. Liu, W. Kong, J. Liu, Y. Liu, L. Zhou, X. Zhang, S.-T. Lee, Z. Kang, Carbon quantum dots with photo-generated proton property as efficient visible light controlled acid catalyst. *Nanoscale* **6**, 867–873 (2014). doi:[10.1039/C3NR03996J](https://doi.org/10.1039/C3NR03996J)
25. M. Kitano, K. Nakajima, J.N. Kondo, S. Hayashi, M. Hara, In vitro reconstitution of mycobacterial ergothioneine biosynthesis. *J. Am. Chem. Soc.* **132**, 6632–6633 (2010). doi:[10.1021/ja101721e](https://doi.org/10.1021/ja101721e)
26. I. Čorić, B. List, Asymmetric spiroacetalization catalysed by confined Brønsted acids. *Nature* **483**, 315 (2012). doi:[10.1038/nature10932](https://doi.org/10.1038/nature10932)
27. H.Z. Liu, T. Jiang, B.X. Han, S.G. Liang, Y.X. Zhou, Selective phenol hydrogenation to cyclohexanone over a dual supported Pd-Lewis acid catalyst. *Science* **326**, 1250 (2009). doi:[10.1126/science.1179713](https://doi.org/10.1126/science.1179713)
28. J.H. Clark, Solid acids for green chemistry. *Acc. Chem. Res.* **35**, 791 (2002). doi:[10.1021/ar010072a](https://doi.org/10.1021/ar010072a)
29. A. Corma, From microporous to mesoporous molecular sieve materials and their use in catalysis. *Chem. Rev.* **97**, 2373 (1997). doi:[10.1021/cr960406n](https://doi.org/10.1021/cr960406n)
30. P. Chen, Solid acid catalysts: stain and shine. *Nat. Chem.* **3**, 839 (2011). doi:[10.1038/nchem.1183](https://doi.org/10.1038/nchem.1183)
31. R.A. Sheldon, R.S. Downing, Heterogeneous catalytic transformations for environmentally friendly production. *Appl. Catal. A* **189**, 163–183 (1999). doi:[10.1016/S0926-860X\(99\)00274-4](https://doi.org/10.1016/S0926-860X(99)00274-4)
32. T. Okuhara, Water-Tolerant solid acid catalysts. *Chem. Rev.* **102**, 3641 (2002). doi:[10.1021/cr0103569](https://doi.org/10.1021/cr0103569)
33. S.K. Yang, W.P. Cai, H.W. Zhang, H.B. Zeng, Y. Lei, A general strategy for fabricating unique carbide nanostructures with excitation wavelength-dependent light emissions. *J. Phys. Chem. C* **15**, 7279–7284 (2011). doi:[10.1021/jp111873k](https://doi.org/10.1021/jp111873k)
34. D.A. Nicewicz, D.W.C. MacMillan, Merging photoredox catalysis with organocatalysis: the direct asymmetric alkylation of aldehydes. *Science* **322**, 77 (2008). doi:[10.1126/science.1161976](https://doi.org/10.1126/science.1161976)
35. M.A. Ischay, M.E. Anzovino, J. Du, T.P. Yoon, Efficient visible light photocatalysis of [2+2] enone cycloadditions. *J. Am. Chem. Soc.* **130**, 12886 (2008). doi:[10.1021/ja805387f](https://doi.org/10.1021/ja805387f)
36. J.M.R. Narayanam, J.W. Tucker, C.R. Stephenson, Electron-transfer photoredox catalysis: development of a tin-free reductive dehalogenation reaction. *J. Am. Chem. Soc.* **131**, 8756 (2009). doi:[10.1021/ja9033582](https://doi.org/10.1021/ja9033582)
37. F.Z. Su, S.C. Mathew, G. Lipner, X.Z. Fu, M. Antonietti, S. Blechert, X.C. Wang, mpg-C3N4-catalyzed selective oxidation of alcohols Using O₂ and visible light. *J. Am. Chem. Soc.* **132**, 16299 (2010). doi:[10.1021/ja102866p](https://doi.org/10.1021/ja102866p)
38. K. Nakajima, M. Hara, Amorphous carbon with SO₃H Groups as a solid Brønsted acid catalyst. *ACS Catal.* **2**, 1296 (2012). doi:[10.1021/cs300103k](https://doi.org/10.1021/cs300103k)
39. F.J. Liu, J. Sun, L.F. Zhu, X.J. Meng, C.Z. Qi, F.-S. Xiao, Sulfated graphene as an efficient solid catalyst for acid-catalyzed liquid reactions. *J. Mater. Chem.* **22**, 5495 (2012). doi:[10.1039/C2JM16608A](https://doi.org/10.1039/C2JM16608A)
40. H.T. Li, X.D. He, Z.H. Kang, H. Huang, Y. Liu, J.L. Liu, S.Y. Lian, C.H.A. Tsang, X.B. Yang, S.T. Lee, Water-soluble fluorescent carbon quantum dots and catalyst design. *Angew. Chem. Int. Ed.* **49**, 4430–4434 (2010). doi:[10.1002/anie.200906154](https://doi.org/10.1002/anie.200906154)

41. Y.Z. Han, H. Huang, H.C. Zhang, Y. Liu, X. Han, R.H. Liu, H.T. Li, Z.H. Kang, Carbon quantum dots with photoenhanced hydrogen-bond catalytic activity in aldol condensations. *ACS Catal.* **4**(3), 781–787 (2014). doi:[10.1021/cs401118x](https://doi.org/10.1021/cs401118x)
42. R.R. Knowles, E.N. Jacobsen, Attractive noncovalent interactions in asymmetric catalysis: links between enzymes and small molecule catalysts. *Proc. Natl. Acad. Sci. U.S.A.* **107**, 20678–20685 (2010). doi:[10.1073/pnas.1006402107](https://doi.org/10.1073/pnas.1006402107)
43. P.R. Carlier, Threading the needle: Mimicking natural toroidal catalysts. *Angew. Chem. Int. Ed.* **43**(20), 2602–2605 (2004). doi:[10.1002/anie.200301731](https://doi.org/10.1002/anie.200301731)
44. P.I. Dalko, L. Moisan, In the golden age of organocatalysis. *Angew. Chem. Int. Ed.* **43**, 5138–5175 (2004). doi:[10.1002/anie.200400650](https://doi.org/10.1002/anie.200400650)
45. T. Akiyama, J. Itoh, K. Yokota, K. Fuchibe, Enantioselective Mannich-type reaction catalyzed by a Chiral Brønsted acid. *Angew. Chem. Int. Ed.* **43**, 1566–1568 (2004). doi:[10.1002/anie.200353240](https://doi.org/10.1002/anie.200353240)
46. V.B. Gondi, M. Gravel, V.H. Rawal, Hydrogen bond catalyzed enantioselective vinylogous Mukaiyama aldol reaction. *Org. Lett.* **7**, 5657–5660 (2005). doi:[10.1021/ol052301p](https://doi.org/10.1021/ol052301p)
47. M.S. Sigman, P. Vachal, E.N. Jacobsen, A general catalyst for the asymmetric Strecker reaction. *Angew. Chem. Int. Ed.* **39**, 1279–1281 (2000). doi:[10.1002/\(SICI\)1521-3773\(20000403\)39:7<1279:AID-ANIE1279>3.0.CO;2-U](https://doi.org/10.1002/(SICI)1521-3773(20000403)39:7<1279:AID-ANIE1279>3.0.CO;2-U)
48. T. Okino, Y. Hoashi, Y. Takemoto, Enantioselective Michael reaction of malonates to nitroolefins catalyzed by bifunctional organocatalysts. *J. Am. Chem. Soc.* **125**, 12672–12673 (2003). doi:[10.1021/ja036972z](https://doi.org/10.1021/ja036972z)
49. B.M. Nugent, R.A. Yoder, J.N. Johnston, Chiral proton catalysis: a catalytic enantioselective direct Aza-Henry reaction. *J. Am. Chem. Soc.* **126**, 3418–3419 (2004). doi:[10.1021/ja031906i](https://doi.org/10.1021/ja031906i)
50. D. Uraguchi, M. Terada, Chiral Brønsted acid-catalyzed direct Mannich reactions via electrophilic activation. *J. Am. Chem. Soc.* **126**, 5356–5367 (2004). doi:[10.1021/ja0491533](https://doi.org/10.1021/ja0491533)
51. Y. Huang, A.K. Unni, A.N. Thadani, V.H. Rawal, Hydrogen bonding: single enantiomers from a chiral-alcohol catalyst. *Nature* **424**, 146 (2003). doi:[10.1038/424146a](https://doi.org/10.1038/424146a)
52. A.K. Unni, N. Takenaka, H. Yamamoto, V.H. Rawal, Axially chiral biaryl diols catalyze highly enantioselective hetero-Diels–Alder reactions through hydrogen bonding. *J. Am. Chem. Soc.* **127**, 1336–1337 (2005). doi:[10.1021/ja044076x](https://doi.org/10.1021/ja044076x)
53. Y. Hoashi, T. Okino, Y. Takemoto, Enantioselective Michael addition to α , β -unsaturated Imides catalyzed by a bifunctional organocatalyst. *Angew. Chem. Int. Ed.* **44**(26), 4032–4035 (2005). doi:[10.1002/anie.200500459](https://doi.org/10.1002/anie.200500459)
54. S. Rajaram, M.S. Sigman, Design of hydrogen bond catalysts based on a modular oxazoline template: application to an enantioselective hetero Diels–Alder reaction. *Org. Lett.* **7**, 5473–5475 (2005). doi:[10.1021/ol052300x](https://doi.org/10.1021/ol052300x)
55. M.S. Sigman, P. Vachal, E.N. Jacobsen, A general catalyst for the asymmetric Strecker reaction. *Angew. Chem. Int. Ed.* **39**(7), 1279–1281 (2000). doi:[10.1002/\(SICI\)1521-3773\(20000403\)39:7<1279:AID-ANIE1279>3.0.CO;2-U](https://doi.org/10.1002/(SICI)1521-3773(20000403)39:7<1279:AID-ANIE1279>3.0.CO;2-U)
56. A.G. Wenzel, E.N. Jacobsen, Asymmetric catalytic Mannich reactions catalyzed by urea derivatives: enantioselective synthesis of β -Aryl- β -amino acids. *J. Am. Chem. Soc.* **124**, 12964–12965 (2002). doi:[10.1021/ja028353g](https://doi.org/10.1021/ja028353g)
57. T. Akiyama, J. Itoh, K. Yokota, K. Fuchibe, Enantioselective Mannich-type reaction catalyzed by a Chiral Brønsted acid. *Angew. Chem. Int. Ed.* **43**(12), 1566–1568 (2004). doi:[10.1002/anie.200353240](https://doi.org/10.1002/anie.200353240)
58. J.D. McGilvra, A.K. Unni, K. Modi, V.H. Rawal, Highly diastereo- and enantioselective Mukaiyama Aldol reactions catalyzed by hydrogen bonding. *Angew. Chem. Int. Ed.* **45**, 6130–6133 (2006). doi:[10.1002/ange.200601638](https://doi.org/10.1002/ange.200601638)
59. A.G. Doyle, E.N. Jacobsen, Small-molecule H-bond donors in asymmetric catalysis. *Chem. Rev.* **107**, 5713–5743 (2007). doi:[10.1021/cr068373r](https://doi.org/10.1021/cr068373r)
60. T.R. Kelly, P. Meghani, V.S. Ekkundi, Diels-alder reactions: rate acceleration promoted by a biphenylenediol. *Tetrahedron Lett.* **31**(24), 3381–3384 (1990). doi:[10.1016/S0040-4039\(00\)97402-1](https://doi.org/10.1016/S0040-4039(00)97402-1)

61. N. Momiyama, H. Yamamoto, Brønsted acid catalysis of achiral enamine for regio- and enantioselective nitroso aldol synthesis. *J. Am. Chem. Soc.* **127**, 1080–1081 (2005). doi:[10.1021/ja0444637](https://doi.org/10.1021/ja0444637)
62. F. Niu, J.Y. Wu, L.S. Zhang, P. Li, J.F. Zhu, Z.Y. Wu, C.R. Wang, W.-G. Song, Hydroxyl group rich C₆₀ fullerene: an excellent hydrogen bond catalyst with superb activity, selectivity, and stability. *ACS Catal.* **1**, 1158–1161 (2011). doi:[10.1021/cs200317d](https://doi.org/10.1021/cs200317d)
63. N.T. McDougal, S.E. Schaus, Asymmetric Morita–Baylis–Hillman reactions catalyzed by Chiral Brønsted acids. *J. Am. Chem. Soc.* **125**, 12094–12095 (2003). doi:[10.1021/ja037705w](https://doi.org/10.1021/ja037705w)
64. F. Niu, C.C. Liu, Z.M. Cui, J. Zhai, L. Jiang, W.-G. Song, Promotion of organic reactions by interfacial hydrogen bonds on hydroxyl group rich nano-solids. *Chem. Commun.* **24**, 2803–2805 (2008). doi:[10.1039/B801361F](https://doi.org/10.1039/B801361F)
65. F. Niu, J. Zhai, L. Jiang, W.-G. Song, Light induced activity switch in interfacial hydrogen-bond catalysis with photo sensitive metal oxides. *Chem. Commun.* **31**, 4738–4740 (2009). doi:[10.1039/B908834B](https://doi.org/10.1039/B908834B)
66. F. Niu, L. Zhang, S.Z. Luo, W.-G. Song, Room temperature aldol reactions using magnetic Fe₃O₄@Fe(OH)₃ composite microspheres in hydrogen bond catalysis. *Chem. Commun.* **46**, 1109–1111 (2010). doi:[10.1039/B920009F](https://doi.org/10.1039/B920009F)
67. L. Cao, S. Sahu, P. Anilkumar, C.E. Bunker, J. Xu, K.A. Shiral Fernando, P. Wang, E.A. Gulians, K.N. Tackett, Y.-P. Sun, Carbon nanoparticles as visible-light photocatalysts for efficient CO₂ conversion and beyond. *J. Am. Chem. Soc.* **133**, 4754–4757 (2011). doi:[10.1021/ja200804h](https://doi.org/10.1021/ja200804h)
68. P. Usubharatana, D. McMartin, A. Veawab, P. Tontiwachwuthikul, Photocatalytic process for CO₂ emission reduction from industrial flue gas streams. *Ind. Eng. Chem. Res.* **45**, 2558–2568 (2006). doi:[10.1021/ie0505763](https://doi.org/10.1021/ie0505763)
69. S.C. Roy, O.K. Varghese, M. Paulose, C.A. Grimes, Toward solar fuels: photocatalytic conversion of carbon dioxide to hydrocarbons. *ACS Nano* **4**, 1259–1278 (2010). doi:[10.1021/nn9015423](https://doi.org/10.1021/nn9015423)
70. X. Chen, S. Shen, L. Guo, S.S. Mao, Semiconductor-based photocatalytic hydrogen generation. *Chem. Rev.* **110**, 6503–6570 (2010). doi:[10.1021/cr1001645](https://doi.org/10.1021/cr1001645)
71. K. Maeda, M. Eguchi, W.J. Youngblood, T.E. Mallouk, Niobium oxide nanoscrolls as building blocks for dye-sensitized hydrogen production from water under visible light irradiation. *Chem. Mater.* **20**, 6770 (2008). doi:[10.1021/cm801807b](https://doi.org/10.1021/cm801807b)
72. X. Wang, L. Cao, F. Lu, M.J. Meziani, H. Li, G. Qi, B. Zhou, B.A. Harruff, Y.-P. Sun, Photoinduced electron transfers with carbon dots. *Chem. Commun.* 3774–3776 (2009). doi:[10.1039/B906252A](https://doi.org/10.1039/B906252A)
73. X. Wang, L. Cao, S.-T. Yang, F. Lu, M.J. Meziani, L. Tian, K.W. Sun, M.A. Bloodgood, Y.-P. Sun, Bandgap-like strong fluorescence in functionalized carbon nanoparticles. *Angew. Chem. Int. Ed.* **49**, 5310–5314 (2010). doi:[10.1002/ange.201000982](https://doi.org/10.1002/ange.201000982)
74. Q.H. Zhang, W.D. Han, Y.J. Hong, J.G. Yu, Photocatalytic reduction of CO₂ with H₂O on Pt-loaded TiO₂ catalyst. *Catal. Today* **148**, 335–340 (2009). doi:[10.1016/j.cattod.2009.07.081](https://doi.org/10.1016/j.cattod.2009.07.081)
75. M.A. Fox, M.T. Dulay, Heterogeneous photocatalysis. *Chem. Rev.* **93**, 341–357 (1993). doi:[10.1021/cr00017a016](https://doi.org/10.1021/cr00017a016)
76. P. Pathak, M.J. Meziani, L. Castillo, Y.-P. Sun, Metal-coated nanoscale TiO₂ catalysts for enhanced CO₂ photoreduction. *Green Chem.* **7**, 667–670 (2005). doi:[10.1039/B507103H](https://doi.org/10.1039/B507103H)
77. H. Yan, J. Yang, G. Ma, G. Wu, X. Zong, Z. Lei, J. Shi, C. Li, Effect of post-calcination on photocatalytic activity of (Ga_{1-x}Zn_x)(N_{1-x}O_x) solid solution for overall water splitting under visible light. *J. Catal.* **254**, 198–204 (2008). doi:[10.1016/j.jcat.2007.12.009](https://doi.org/10.1016/j.jcat.2007.12.009)
78. K. Maeda, K. Domen, Photocatalytic water splitting: recent progress and future challenges. *J. Phys. Chem. Lett.* **1**, 2655–2661 (2010). doi:[10.1021/jz1007966](https://doi.org/10.1021/jz1007966)
79. T.-F. Yeh, C.-Y. Teng, S.-J. Chen, H. Teng, Nitrogen-doped graphene oxide quantum dots as photocatalysts for overall water-splitting under visible light illumination. *Adv. Mater.* **26**, 3297–3303 (2014). doi:[10.1002/adma.201305299](https://doi.org/10.1002/adma.201305299)

80. T.F. Yeh, S.J. Chen, C.S. Yeh, H. Teng, Tuning the electronic structure of graphite oxide through ammonia treatment for photocatalytic generation of H₂ and O₂ from water splitting. *J. Phys. Chem. C* **117**, 6516–6524 (2013). doi:[10.1021/jp312613r](https://doi.org/10.1021/jp312613r)
81. G. Eda, Y.Y. Lin, C. Mattevi, H. Yamaguchi, H.A. Chen, I.S. Chen, C.W. Chen, M. Chhowalla, Blue photoluminescence from chemically derived graphene oxide. *Adv. Mater.* **22**, 505–509 (2010). doi:[10.1002/adma.200901996](https://doi.org/10.1002/adma.200901996)
82. H. Tetsuka, R. Asahi, A. Nagoya, K. Okamoto, I. Tajima, R. Ohta, A. Okamoto, Optically tunable amino-functionalized graphene quantum dots. *Adv. Mater.* **24**, 5333–5338 (2012). doi:[10.1002/adma.201201930](https://doi.org/10.1002/adma.201201930)
83. S.H. Jin, D.H. Kim, G.H. Jun, S.H. Hong, S. Jeon, Tuning the photoluminescence of graphene quantum dots through the charge transfer effect of functional groups. *ACS Nano* **7**, 1239–1245 (2013). doi:[10.1021/nn304675g](https://doi.org/10.1021/nn304675g)
84. L.A. Ponomarenko, F. Schedin, M.I. Katsnelson, R. Yang, E.W. Hill, K.S. Novoselov, Chaotic Dirac billiard in graphene quantum dots. *Science* **320**, 356–358 (2008). doi:[10.1126/science.1154663](https://doi.org/10.1126/science.1154663)
85. Y.W. Son, M.L. Cohen, S.G. Louie, Energy gaps in graphene nanoribbons. *Phys. Rev. Lett.* **97**, 216803 (2006). doi:[10.1103/PhysRevLett.97.216803](https://doi.org/10.1103/PhysRevLett.97.216803)
86. X. Li, X. Wang, L. Zhang, S. Lee, H. Dai, Chemically derived, ultrasoft graphene nanoribbon semiconductors. *Science* **319**, 1229–1232 (2008). doi:[10.1126/science.1150878](https://doi.org/10.1126/science.1150878)
87. S.B. Yang, X.L. Feng, X.C. Wang, K. Müllen, Graphene-based carbon nitride nanosheets as efficient metal-free electrocatalysts for oxygen reduction reactions. *Angew. Chem. Int. Ed.* **50**, 5339–5343 (2011). doi:[10.1002/anie.201100170](https://doi.org/10.1002/anie.201100170)
88. Y. Li, Y. Zhao, H.H. Cheng, Y. Hu, G.Q. Shi, L.M. Dai, L.T. Qu, Nitrogen-doped graphene quantum dots with oxygen-rich functional groups. *J. Am. Chem. Soc.* **134**, 15–18 (2012). doi:[10.1021/ja206030c](https://doi.org/10.1021/ja206030c)
89. R. Yan, H. Wu, Q. Zheng, J.Y. Wang, J.L. Huang, K.J. Ding, Q.G. Guo, J.Z. Wang, Graphene quantum dots cut from graphene flakes: high electrocatalytic activity for oxygen reduction and low cytotoxicity. *RSC Adv.* **4**, 23097–23106 (2014). doi:[10.1039/C4RA02336F](https://doi.org/10.1039/C4RA02336F)
90. Y. Liu, P.Y. Wu, Graphene quantum dot hybrids as efficient metal-free electrocatalyst for the oxygen reduction reaction. *ACS Appl. Mater. Interfaces* **5**, 3362–3369 (2013). doi:[10.1021/am400415t](https://doi.org/10.1021/am400415t)
91. W.A. Saidi, Oxygen reduction electrocatalysis using N-doped graphene quantum-dots. *J. Phys. Chem. Lett.* **4**, 4160–4165 (2013). doi:[10.1021/jz402090d](https://doi.org/10.1021/jz402090d)
92. C.Z. Zhu, J.F. Zhai, S.J. Dong, Bifunctional fluorescent carbon nanodots: green synthesis via soy milk and application as metal-free electrocatalysts for oxygen reduction. *Chem. Commun.* **48**, 9367–9369 (2012). doi:[10.1039/C2CC33844K](https://doi.org/10.1039/C2CC33844K)
93. L. Zhou, J. Liu, X. Zhang, R. Liu, H. Huang, Y. Liu, Z. Kang, Template-free fabrication of mesoporous carbons from carbon quantum dots and their catalytic application to the selective oxidation of hydrocarbons. *Nanoscale* **6**, 5831–5837 (2014). doi:[10.1039/C4NR00716F](https://doi.org/10.1039/C4NR00716F)
94. G.A. Ozin, Nanochemistry: synthesis in diminishing dimensions. *Adv. Mater.* **4**, 612–649 (1992). doi:[10.1002/adma.19920041003](https://doi.org/10.1002/adma.19920041003)
95. A. Mehdi, C. Reye, R. Corriu, From molecular chemistry to hybrid nanomaterials. Design and functionalization. *Chem. Soc. Rev.* **40**, 563–574 (2011). doi:[10.1039/B920516K](https://doi.org/10.1039/B920516K)
96. D.H. Zhang, C. Zhou, Z.H. Sun, L.-Z. Wu, C.-H. Tung, T.R. Zhang, Magnetically recyclable nanocatalysts (MRNCs): a versatile integration of high catalytic activity and facile recovery. *Nanoscale* **4**, 6244–6255 (2012). doi:[10.1039/C2NR31929B](https://doi.org/10.1039/C2NR31929B)
97. R.H. Baughman, A.A. Zakhidov, W.A. de Heer, Carbon nanotubes—the route toward applications. *Science* **297**, 787–792 (2002). doi:[10.1126/science.1060928](https://doi.org/10.1126/science.1060928)
98. Y.W. Zhu, S. Murali, W.W. Cai, X.S. Li, J.W. Suk, J.R. Potts, R.S. Ruoff, Graphene and graphene oxide: synthesis, properties, and applications. *Adv. Mater.* **22**, 3906–3924 (2010). doi:[10.1002/adma.201001068](https://doi.org/10.1002/adma.201001068)

99. G. Williams, B. Seger, P.V. Kamat, TiO₂-graphene nanocomposites. UV-assisted photocatalytic reduction of graphene oxide. *ACS Nano* **2**, 1487–1491 (2008). doi:[10.1021/mn800251f](https://doi.org/10.1021/mn800251f)
100. T. Rueckes, K. Kim, E. Joselevich, G.Y. Tseng, C.-L. Cheung, C.M. Lieber, Carbon nanotube-based nonvolatile random access memory of molecular computing. *Science* **289**, 94–97 (2000). doi:[10.1126/science.289.5476.94](https://doi.org/10.1126/science.289.5476.94)
101. B.Z. Fang, H.S. Zhou, I. Honma, Ordered porous carbon with tailored pore size for electrochemical hydrogen storage application. *J. Phys. Chem. B* **110**, 4875–4880 (2006). doi:[10.1021/jp056063r](https://doi.org/10.1021/jp056063r)
102. H.L. Wang, Q.M. Gao, J. Hu, High hydrogen storage capacity of porous carbons prepared by using activated carbon. *J. Am. Chem. Soc.* **131**, 7016–7022 (2009). doi:[10.1021/ja8083225](https://doi.org/10.1021/ja8083225)
103. M. Hartmann, A. Vinu, G. Chandrasekar, Adsorption of Vitamin E on mesoporous carbon molecular sieves. *Chem. Mater.* **17**, 829–833 (2005). doi:[10.1021/cm048564f](https://doi.org/10.1021/cm048564f)
104. J.-S. Yu, S. Kang, S.B. Yoon, G. Chai, Fabrication of ordered uniform porous carbon networks and their application to a catalyst supporter. *J. Am. Chem. Soc.* **124**, 9382–9383 (2002). doi:[10.1021/ja0203972](https://doi.org/10.1021/ja0203972)
105. S.L. Zhang, L. Chen, S.X. Zhou, D.Y. Zhao, L.M. Wu, Facile synthesis of hierarchically ordered porous carbon via in situ self-assembly of colloidal polymer and silica spheres and its use as a catalyst support. *Chem. Mater.* **22**, 3433–3440 (2010). doi:[10.1021/cm1002274](https://doi.org/10.1021/cm1002274)
106. F.B. Su, J.H. Zeng, X.Y. Bao, Y.S. Yu, J.Y. Lee, X.S. Zhao, Preparation and characterization of highly ordered graphitic mesoporous carbon as a Pt catalyst support for direct methanol fuel cells. *Chem. Mater.* **17**, 3960–3967 (2005). doi:[10.1021/cm0502222](https://doi.org/10.1021/cm0502222)
107. K.X. Wang, Y.G. Wang, Y.R. Wang, E. Hosono, H.S. Zhou, Mesoporous carbon nanofibers for supercapacitor application. *J. Phys. Chem. C* **113**, 1093–1097 (2008). doi:[10.1021/jp807463u](https://doi.org/10.1021/jp807463u)
108. S. Oh, K. Kim, Synthesis of a new mesoporous carbon and its application to electrochemical double-layer capacitors. *Chem. Commun.* 2177–2178 (1999). doi:[10.1039/A906872D](https://doi.org/10.1039/A906872D)
109. T. Kyotani, Z.X. Ma, A. Tomita, Template synthesis of novel porous carbons using various types of zeolites. *Carbon* **41**, 1451–1459 (2003). doi:[10.1016/S0008-6223\(03\)00090-3](https://doi.org/10.1016/S0008-6223(03)00090-3)
110. Y.D. Xia, R. Mokaya, Ordered mesoporous carbon monoliths: CVD nanocasting and hydrogen storage properties. *J. Phys. Chem. C* **111**, 10035–10039 (2007). doi:[10.1021/jp071936y](https://doi.org/10.1021/jp071936y)
111. R.H. Liu, H. Huang, H.T. Li, Y. Liu, J. Zhong, Y.Y. Li, S. Zhang, Z.H. Kang, Metal nanoparticle/carbon quantum dot composite as a photocatalyst for high-efficiency cyclohexane oxidation. *ACS Catalysis* **1**, 328–336 (2014). doi:[10.1021/cs400913h](https://doi.org/10.1021/cs400913h)
112. H. Hattori, Y. Ide, S. Ogo, K. Inumaru, M. Sadakane, Sano, efficient and selective photocatalytic cyclohexane oxidation on a layered titanate modified with iron oxide under sunlight and CO₂ atmosphere. *T. ACS Catal.* **2**, 1910–1915 (2012). doi:[10.1021/cs300339f](https://doi.org/10.1021/cs300339f)
113. C.H. Wang, L.F. Chen, Z.W. Qi, One-pot synthesis of gold nanoparticles embedded in silica for cyclohexane oxidation. *Catal. Sci. Technol.* **3**, 1123–1128 (2013). doi:[10.1039/C2CY20692G](https://doi.org/10.1039/C2CY20692G)
114. D. Bonnet, T. Ireland, E. Fache, J.-P. Simonato, Innovative direct synthesis of adipic acid by air oxidation of cyclohexane. *Green Chem.* **8**, 556–559 (2006). doi:[10.1039/B600903D](https://doi.org/10.1039/B600903D)
115. M.S. Hamdy, A. Ramanathan, T. Maschmeyer, U. Hanefeld, J.C. Jansen, Co-TUD-1: a ketone-selective catalyst for cyclohexane oxidation. *Chem. Eur. J.* **12**, 1782–1789 (2006). doi:[10.1002/chem.200500166](https://doi.org/10.1002/chem.200500166)
116. U. Pillai, R.E. Sahle-Demessie, A highly efficient oxidation of cyclohexane over Au/ZSM-5 molecular sieve catalyst with oxygen as oxidant. *Chem. Commun.* **0**, 2142–2143 (2002). doi:[10.1039/B315098D](https://doi.org/10.1039/B315098D)
117. F.A. Chavez, C.V. Nguyen, M.M. Olmstead, P.K. Mascharak, Synthesis, properties, and structure of a stable cobalt(III) alkyl peroxide complex and its role in the oxidation of cyclohexane. *Inorg. Chem.* **35**, 6282–6291 (1996). doi:[10.1021/ic960500m](https://doi.org/10.1021/ic960500m)

118. P. Comba, M. Maurer, P. Vadivelu, Oxidation of cyclohexane by high-valent iron bispidine complexes: tetradentate versus pentadentate ligands. *Inorg. Chem.* **48**, 10389–10396 (2009). doi:[10.1021/ic901702s](https://doi.org/10.1021/ic901702s)
119. A.S. Goldstein, R.H. Beer, R.S. Drago, Catalytic oxidation of hydrocarbons with O₂ or H₂O₂ using a sterically hindered ruthenium complex. *J. Am. Chem. Soc.* **116**, 2424–2429 (1994). doi:[10.1021/ja00085a023](https://doi.org/10.1021/ja00085a023)
120. S.-M. Yiu, W.-L. Man, T.-C. Lau, Efficient catalytic oxidation of alkanes by Lewis acid/[Os^{VI}(N)Cl₄][−] using peroxides as terminal oxidants. Evidence for a metal-based active intermediate. *J. Am. Chem. Soc.* **130**, 10821–10827 (2008). doi:[10.1021/ja802625e](https://doi.org/10.1021/ja802625e)
121. V.I. Părvulescu, D. Dumitriu, G. Poncelet, Hydrocarbons oxidation with hydrogen peroxide over germanic faujasites catalysts. *Catal. A-Chem.* **140**, 91–105 (1999). doi:[10.1016/S1381-1169\(98\)00221-0](https://doi.org/10.1016/S1381-1169(98)00221-0)
122. E.V. Spinacé, H.O. Pastore, U. Schuchardt, Cyclohexane oxidation catalyzed by titanium silicalite(TS-1): overoxidation and comparison with other oxidation systems. *J. Catal.* **157**, 631–635 (1995). doi:[10.1006/jcat.1995.1328](https://doi.org/10.1006/jcat.1995.1328)
123. G.M. Lü, D. Ji, G. Qian, Y.X. Qi, X.L. Wang, J.S. Suo, Gold nanoparticles in mesoporous materials showing catalytic selective oxidation cyclohexane using oxygen. *Appl. Catal. A* **280**, 175–180 (2005). doi:[10.1016/j.apcata.2004.10.034](https://doi.org/10.1016/j.apcata.2004.10.034)
124. R. Raja, G. Sankar, J.M. Thomas, Powerful redox molecular sieve catalysts for the selective oxidation of cyclohexane in air. *J. Am. Chem. Soc.* **121**, 11926–11927 (1999). doi:[10.1021/ja9935052](https://doi.org/10.1021/ja9935052)
125. Y. Yuan, H.B. Ji, Y.X. Chen, Y. Han, X.F. Song, Y.B. She, R.G. Zhong, Oxidation of cyclohexane to adipic acid using Fe-porphyrin as a biomimetic catalyst. *Org. Process Res. Dev.* **8**, 418–420 (2004). doi:[10.1021/op049974s](https://doi.org/10.1021/op049974s)
126. B. Sarkar, P. Prajapati, R. Tiwari, S. Ghosh, S.S. Acharyya, C. Pendem, R.K. Singha, L.N.S. Konathala, J. Kumar, T. Sasaki, R. Bal, Room temperature selective oxidation of cyclohexane over Cu-nanoclusters supported on nanocrystalline Cr₂O₃. *Green Chem.* **14**, 2600–2606 (2012). doi:[10.1039/C2GC35658A](https://doi.org/10.1039/C2GC35658A)
127. A. Wittstock, V. Zielasek, J. Biener, C.M. Friend, M. Bäumer, Nanoporous gold catalysts for selective gas-phase oxidative coupling of methanol at low temperature. *Science* **327**, 319–322 (2010). doi:[10.1126/science.1183591](https://doi.org/10.1126/science.1183591)
128. J.L. Gu, Y.L. Gu, Y. Huang, S.P. Elangovan, Y.S. Li, W.R. Zhao, I. Toshio, Y. Yamazaki, J.L. Shi, Highly dispersed copper species within SBA-15 introduced by the hydrophobic core of a surfactant micelle as a carrier and their enhanced catalytic activity for cyclohexane oxidation. *J. Phys. Chem. C* **115**, 21211–21217 (2011). doi:[10.1021/jp206132a](https://doi.org/10.1021/jp206132a)
129. K.-I. Shimizu, Y. Murata, A. Satsuma, Dicopper(II)–Dioxygen complexes in Y zeolite for selective catalytic oxidation of cyclohexane under photoirradiation. *J. Phys. Chem. C* **111**, 19043–19051 (2007). doi:[10.1021/jp0767821](https://doi.org/10.1021/jp0767821)
130. S.S. Shankar, A. Rai, A. Ahmad, M. Sastry, Rapid synthesis of Au, Ag and bimetallic Au-shell nanoparticles using Neem. *J. Colloid Interf. Sci.* **275**, 496–502 (2004). doi:[10.1016/j.jcis.2004.03.003](https://doi.org/10.1016/j.jcis.2004.03.003)
131. J. Liu, H.C. Zhang, D. Tang, X. Zhang, L.K. Yan, Y.Z. Han, H. Huang, Y. Liu, Z.H. Kang, Carbon quantum dot/silver nanoparticle/polyoxometalate composites as photocatalysts for overall water splitting in visible light. *ChemCatChem* **6**, 2634–2641 (2014). doi:[10.1002/cctc.201402227](https://doi.org/10.1002/cctc.201402227)
132. A. Fujishima, K. Honda, Electrochemical photolysis of water at a semiconductor electrode. *Nature* **238**, 37–38 (1972). doi:[10.1038/238037a0](https://doi.org/10.1038/238037a0)
133. A. Iwase, Y.H. Ng, Y. Ishiguro, A. Kudo, R. Amal, Reduced graphene oxide as a solid-state electron mediator in Z-scheme photocatalytic water splitting under visible light. *J. Am. Chem. Soc.* **133**, 11054–11057 (2011). doi:[10.1021/ja203296z](https://doi.org/10.1021/ja203296z)
134. H.G. Kim, P.H. Borse, J.S. Jang, C.W. Ahn, E.D. Jeong, J.S. Lee, Engineered nanorod perovskite film photocatalysts to harvest visible light. *Adv. Mater.* **23**, 2088–2092 (2011). doi:[10.1002/adma.201004171](https://doi.org/10.1002/adma.201004171)

135. A. Mukherji, R. Marschall, A. Tanksale, C. Sun, S.C. Smith, G.Q. Lu, L. Wang, N-doped CsTaWO₆ as a new photocatalyst for hydrogen production from water splitting under solar irradiation. *Adv. Funct. Mater.* **21**, 126–132 (2011). doi:[10.1002/adfm.201000591](https://doi.org/10.1002/adfm.201000591)
136. Y. Liu, H. Ming, Z. Ma, H. Huang, S.Y. Lian, H.T. Li, X.D. He, H. Yu, K.M. Pan, Z.H. Kang, Nanoporous TiO₂ spheres with narrow pore size distribution and improved visible light photocatalytic abilities. *Chem. Commun.* **47**, 8025–8027 (2011). doi:[10.1039/C1CC12557E](https://doi.org/10.1039/C1CC12557E)
137. K. Maeda et al., Photocatalytic overall water splitting promoted by two different cocatalysts for hydrogen and oxygen evolution under visible light. *Angew. Chem.* **122**, 4190–4193 (2010). doi:[10.1002/ange.201001259](https://doi.org/10.1002/ange.201001259)
138. H. Zhang, G. Chen, X. He, Y. Li, Electronic structure and water splitting under visible-light irradiation of Zn and Ag co-doped In(OH)_yS_z photocatalysts. *Int. J. Hydrogen Energy* **37**, 5532–5539 (2012). doi:[10.1016/j.ijhydene.2011.12.155](https://doi.org/10.1016/j.ijhydene.2011.12.155)
139. A. Kudo, Y. Miseki, Heterogeneous photocatalyst materials for water splitting. *Chem. Soc. Rev.* **38**, 253–278 (2009). doi:[10.1039/B800489G](https://doi.org/10.1039/B800489G)
140. K. Iwashina, A. Kudo, Rh-Doped SrTiO₃ photocatalyst electrode showing cathodic photocurrent for water splitting under visible-light irradiation. *J. Am. Chem. Soc.* **133**, 13272–13275 (2011). doi:[10.1021/ja2050315](https://doi.org/10.1021/ja2050315)
141. R. Abe, M. Higashi, K. Domen, Facile fabrication of an efficient oxynitride TaON photoanode for overall water splitting into H₂ and O₂ under visible light irradiation. *J. Am. Chem. Soc.* **132**, 11828–11829 (2010). doi:[10.1021/ja1016552](https://doi.org/10.1021/ja1016552)
142. G.R. Bamwenda, T. Uesigi, Y. Abe, K. Sayama, H. Arakawa, The photocatalytic oxidation of water to O₂ over pure CeO₂, WO₃, and TiO₂ using Fe³⁺ and Ce⁴⁺ as electron acceptors. *Appl. Catal. A-Gen.* **205**, 117–128 (2001). doi:[10.1016/S0926-860X\(00\)00549-4](https://doi.org/10.1016/S0926-860X(00)00549-4)
143. T. Ohno, L. Bai, T. Hisatomi, K. Maeda, K. Domen, Photocatalytic water splitting using modified GaN:ZnO solid solution under visible light: long-time operation and regeneration of activity. *J. Am. Chem. Soc.* **134**, 8254–8259 (2012). doi:[10.1021/ja302479f](https://doi.org/10.1021/ja302479f)
144. N. Arai, N. Saito, H. Nishiyama, Y. Shimodaira, H. Kohayashi, Y. Inoue, K. Sato, Photocatalytic activity for overall water splitting of RuO₂-loaded Y_xIn_{2-x}O₃ (x = 0.9–1.5). *J. Phys. Chem. C* **112**, 5000–5005 (2008). doi:[10.1021/jp709629t](https://doi.org/10.1021/jp709629t)
145. S.H. Hwang, C. Kim, J. Jang, SnO₂ nanoparticle embedded TiO₂ nanofibers-highly efficient photocatalyst for the degradation of rhodamine B. *Catal. Commun.* **12**, 1037–1041 (2011). doi:[10.1016/j.catcom.2011.02.024](https://doi.org/10.1016/j.catcom.2011.02.024)
146. J. Sato, N. Saito, Y. Yamada, K. Maeda, T. Takata, J.N. Kondo, M. Hara, H. Kobayashi, K. Domen, Y. Inoue, RuO₂-loaded β-Ge₃N₄ as a non-oxide photocatalyst for overall water splitting. *J. Am. Chem. Soc.* **127**, 4150–4151 (2005). doi:[10.1021/ja042973v](https://doi.org/10.1021/ja042973v)
147. K. Maeda, K. Teramura, D. Lu, T. Takata, N. Saito, Y. Inoue, K. Domen, Photocatalyst releasing hydrogen from water-enhancing catalytic performance holds promise for hydrogen production by water splitting in sunlight. *Nature* **440**, 295–295 (2006). doi:[10.1038/440295a](https://doi.org/10.1038/440295a)
148. D. Wang, R. Li, J. Zhu, J. Shi, J. Han, X. Zong, C. Li, Photocatalytic water oxidation on BiVO₄ with the electrocatalyst as an oxidation cocatalyst: essential relations between electrocatalyst and photocatalyst. *J. Phys. Chem. C* **116**, 5082–5089 (2012). doi:[10.1021/jp210584b](https://doi.org/10.1021/jp210584b)
149. D.K. Zhong, S. Choi, D.R. Gamelin, Near-complete suppression of surface recombination in solar photoelectrolysis by “Co-Pi” catalyst-modified W:BiVO₄. *J. Am. Chem. Soc.* **133**, 18370–18377 (2011). doi:[10.1021/ja207348x](https://doi.org/10.1021/ja207348x)
150. S.K. Pilli, T.E. Furtak, L.D. Brown, T.G. Deutsch, J.A. Turner, A.M. Herring, Cobalt-phosphate (Co-Pi) catalyst modified Mo-doped BiVO₄ photoelectrodes for solar water oxidation. *Energy Environ. Sci.* **4**, 5028–5034 (2011). doi:[10.1039/C1EE02444B](https://doi.org/10.1039/C1EE02444B)
151. J.A. Seabold, K.S. Choi, Effect of a cobalt-based oxygen evolution catalyst on the stability and the selectivity of photo-oxidation reactions of a WO₃ photoanode. *Chem. Mater.* **23**, 1105–1112 (2011). doi:[10.1021/cm1019469](https://doi.org/10.1021/cm1019469)

152. K. Sayama, K. Mukasa, R. Abe, Y. Abe, H. Arakawa, A new photocatalytic water splitting system under visible light irradiation mimicking a Z-scheme mechanism in photosynthesis. *J. Photochem. Photobiol. A* **148**, 71–77 (2002). doi:[10.1016/S1010-6030\(02\)00070-9](https://doi.org/10.1016/S1010-6030(02)00070-9)
153. F.M. Toma et al., Efficient water oxidation at carbon nanotube–polyoxometalate electrocatalytic interfaces. *Nat. Chem.* **2**, 826–831 (2010). doi:[10.1038/nchem.761](https://doi.org/10.1038/nchem.761)
154. Z.Y. Zhang, Q.P. Lin, S.T. Zheng, X.H. Bu, P.Y. Feng, A novel sandwich-type polyoxometalate compound with visible-light photocatalytic H₂ evolution activity. *Chem. Commun.* **47**, 3918–3920 (2011). doi:[10.1039/C0CC04697C](https://doi.org/10.1039/C0CC04697C)
155. X. Liu, Y. Li, S. Peng, G. Lu, S. Li, Photocatalytic hydrogen evolution under visible light irradiation by the polyoxometalate α -[AlSiW₁₁(H₂O)O₃₉]⁵⁻–Eosin Y system. *Int. J. Hydrogen Energy* **37**, 12150–12157 (2012). doi:[10.1016/j.ijhydene.2012.06.028](https://doi.org/10.1016/j.ijhydene.2012.06.028)
156. A. Sartorel, P. Miró, E. Salvadori, S. Romain, M. Carraro, G. Scorrano, M.D. Valentin, A. Llobet, C. Bo, M. Bonchio, Water oxidation at a tetraruthenate core stabilized by polyoxometalate ligands: experimental and computational evidence to trace the competent intermediates. *J. Am. Chem. Soc.* **131**, 16051–16053 (2009). doi:[10.1021/ja905067u](https://doi.org/10.1021/ja905067u)
157. B. Nohra et al., Polyoxometalate-based metal organic frameworks (POMOFs): structural trends, energetics, and high electrocatalytic efficiency for hydrogen evolution reaction. *J. Am. Chem. Soc.* **133**, 13363–13374 (2011). doi:[10.1021/ja201165c](https://doi.org/10.1021/ja201165c)
158. A. Sartorel, M. Carraro, G. Scorrano, R.D. Zorzi, S. Geremia, N.D. McDaniel, S. Bernhard, M. Bonchio, Polyoxometalate embedding of a Tetraruthenium(IV)-oxo-core by template-directed metalation of $[\gamma\text{-SiW}_{10}\text{O}_{36}]^{8-}$: a totally inorganic oxygen-evolving catalyst. *J. Am. Chem. Soc.* **130**, 5006–5007 (2008). doi:[10.1021/ja077837f](https://doi.org/10.1021/ja077837f)
159. P.V. Kamat, Photophysical, photochemical and photocatalytic aspects of metal nanoparticles. *J. Phys. Chem. B* **106**, 7729–7744 (2002). doi:[10.1021/jp0209289](https://doi.org/10.1021/jp0209289)
160. S. Hara, M. Yoshimizu, S. Tanigawa, L. Ni, B. Ohtani, H. Irie, Hydrogen and oxygen evolution photocatalysts synthesized from strontium titanate by controlled doping and their performance in two-step overall water splitting under visible light. *J. Phys. Chem. C* **116**, 17458–17463 (2012). doi:[10.1021/jp306315r](https://doi.org/10.1021/jp306315r)
161. C. Costa-Coquelard, S. Sorgues, L. Ruhlmann, Photocatalysis with polyoxometalates associated to porphyrins under visible light: an application of charge transfer in electrostatic complexes. *J. Phys. Chem. A* **114**, 6394–6400 (2010). doi:[10.1021/jp101261n](https://doi.org/10.1021/jp101261n)
162. S. Kim, J. Yeo, W. Choi, Simultaneous conversion of dye and hexavalent chromium in visible light-illuminated aqueous solution of polyoxometalate as an electron transfer catalyst. *Appl. Catal. B* **84**, 148–155 (2008). doi:[10.1016/j.apcatb.2008.03.012](https://doi.org/10.1016/j.apcatb.2008.03.012)
163. P. Wang, B.B. Huang, X.Y. Qin, X.Y. Zhang, Y. Dai, J.Y. Wei, M.-H. Whangbo, Ag@AgCl: a highly efficient and stable photocatalyst active under visible light. *Angew. Chem.* **120**, 8049–8051 (2008). doi:[10.1002/anie.200802483](https://doi.org/10.1002/anie.200802483)
164. M.R. Hoffmann, S.T. Martin, W. Choi, W. Bahnemann, Environmental applications of semiconductor photocatalysis. *Chem. Rev.* **95**, 69–96 (1995). doi:[10.1021/cr00033a004](https://doi.org/10.1021/cr00033a004)
165. A. Müller, F. Peters, M.T. Pope, D. Gatteschi, Polyoxometalates: very large clusters nanoscale magnets. *Chem. Rev.* **98**, 239–272 (1998). doi:[10.1021/cr9603946](https://doi.org/10.1021/cr9603946)
166. J.T. Rhule, C.L. Hill, D.A. Judd, R.F. Schinazi, Polyoxometalates in medicine. *Chem. Rev.* **98**, 327–357 (1998). doi:[10.1021/cr960396q](https://doi.org/10.1021/cr960396q)
167. E. Coronado, C.J. Gómez-García, Polyoxometalate-based molecular materials. *Chem. Rev.* **98**, 273–296 (1998). doi:[10.1021/cr970471c](https://doi.org/10.1021/cr970471c)
168. H. Zhang, H. Huang, H. Ming, H. Li, L. Zhang, Y. Liu, Z.H. Kang, Carbon quantum Dots/Ag₃PO₄ complex photocatalysts with enhanced photocatalytic activity and stability under visible light. *J. Mater. Chem.* **22**, 10501–10506 (2012). doi:[10.1039/C2JM30703K](https://doi.org/10.1039/C2JM30703K)
169. H.T. Li, R.H. Liu, Y. Liu, H. Huang, H. Yu, H. Ming, S.Y. Lian, S.T. Lee, Z.H. Kang, Carbon quantum dots/Cu₂O composites with protruding nanostructures and their highly efficient (near) infrared photocatalytic behavior. *J. Mater. Chem.* **22**, 17470–17475 (2012). doi:[10.1039/C2JM32827E](https://doi.org/10.1039/C2JM32827E)

170. X. Zhang, F. Wang, H. Huang, H. Li, X. Han, Y. Liu, Z. Kang, Carbon quantum dot sensitized TiO₂ nanotube arrays for photoelectrochemical hydrogen generation under visible light†. *Nanoscale* **5**, 2274–2278 (2013). doi:[10.1039/C3NR34142A](https://doi.org/10.1039/C3NR34142A)
171. S. Nishimura, N. Abrams, B.A. Lewis, L.I. Halaoui, T.E. Mallouk, K.D. Benkstein, J. van de Lagemaat, A.J. Frank, Standing wave enhancement of red absorbance and photocurrent in dye-sensitized titanium dioxide photoelectrodes coupled to photonic crystals. *J. Am. Chem. Soc.* **125**, 6306–6310 (2003). doi:[10.1021/ja034650p](https://doi.org/10.1021/ja034650p)
172. L.I. Halaoui, N.M. Abrams, T.E. Mallouk, Increasing the conversion efficiency of dye-sensitized TiO₂ photoelectrochemical cells by coupling to photonic crystals. *J. Phys. Chem. B* **109**, 6334–6342 (2005). doi:[10.1021/jp044228a](https://doi.org/10.1021/jp044228a)
173. W.J. Youngblood, S.H.A. Lee, K. Maeda, T.E. Mallouk, Visible light water splitting using dye-sensitized oxide semiconductors. *Acc. Chem. Res.* **42**, 1966–1972 (2009). doi:[10.1021/ar9002398](https://doi.org/10.1021/ar9002398)
174. W.J. Youngblood, S.H.A. Lee, Y. Kobayashi, E.A. Hernandez-Pagan, P.G. Hoertz, T.A. Moore, A.L. Moore, D. Gust, T.E. Mallouk, Photoassisted overall water splitting in a visible light-absorbing dye-sensitized photoelectrochemical cell. *J. Am. Chem. Soc.* **131**, 926–927 (2009). doi:[10.1021/ja809108y](https://doi.org/10.1021/ja809108y)
175. L. Li, L.L. Duan, Y.H. Xu, M. Gorlov, A. Hagfeldt, L.C. Sun, A photoelectrochemical device for visible light driven water splitting by a molecular ruthenium catalyst assembled on dye-sensitized nanostructured TiO₂. *Chem. Commun.* **46**, 7307–7309 (2010). doi:[10.1039/C0CC01828G](https://doi.org/10.1039/C0CC01828G)
176. G. Calogero, G.D. Marco, S. Caramori, S. Cazzanti, R. Argazzi, C.A. Bignozzi, Natural dye sensitizers for photoelectrochemical cells. *Energy Environ. Sci.* **2**, 1162–1172 (2009). doi:[10.1039/B913248C](https://doi.org/10.1039/B913248C)
177. X.-F. Gao, H.-B. Li, W.-T. Sun, Q. Chen, F.-Q. Tang, L.-M. Peng, CdTe quantum dots-sensitized TiO₂ nanotube array photoelectrodes. *J. Phys. Chem. C* **113**, 7531–7535 (2009). doi:[10.1021/jp810727n](https://doi.org/10.1021/jp810727n)
178. W.T. Sun, Y. Yu, H.Y. Pan, X.F. Gao, Q. Chen, L.M. Peng, CdS quantum dots sensitized TiO₂ nanotube-array photoelectrodes. *J. Am. Chem. Soc.* **130**, 1124–1125 (2008). doi:[10.1021/ja0777741](https://doi.org/10.1021/ja0777741)
179. G.M. Wang, X.Y. Yang, F. Qian, J.Z. Zhang, Y. Li, Double-sided CdS and CdSe quantum dot co-sensitized ZnO nanowire arrays for photoelectrochemical hydrogen generation. *Nano Lett.* **10**, 1088–1092 (2010). doi:[10.1021/nl100250z](https://doi.org/10.1021/nl100250z)
180. J. Hensel, G.M. Wang, Y. Li, J.Z. Zhang, Synergistic effect of CdSe quantum dot sensitization and nitrogen doping of TiO₂ nanostructures for photoelectrochemical solar hydrogen generation. *Nano Lett.* **10**, 478–483 (2010). doi:[10.1021/nl903217w](https://doi.org/10.1021/nl903217w)
181. J.H. Bang, P.V. Kamat, Solar cells by design: photoelectrochemistry of TiO₂ nanorod arrays decorated with CdSe. *Adv. Funct. Mater.* **2010**, 20 (1970). doi:[10.1002/adfm.200902234](https://doi.org/10.1002/adfm.200902234)
182. F. Wang, Y. Zhang, Y. Liu, X. Wang, M. Shen, S.-T. Lee, Z. Kang, Opto-electronic conversion logic behaviour through dynamic modulation of electron/energy transfer states at the TiO₂-carbon quantum dot interface. *Nanoscale* **5**, 1831–1835 (2013). doi:[10.1039/C3NR33985H](https://doi.org/10.1039/C3NR33985H)
183. R. Liu, J. Liu, W. Kong, H. Huang, X. Han, X. Zhang, Y. Liu, Z. Kang, Adsorption dominant catalytic activity of a carbon dots stabilized gold nanoparticles system. *Dalton Trans.* **43**, 10920–10929 (2014). doi:[10.1039/C4DT00630E](https://doi.org/10.1039/C4DT00630E)
184. H.B. Xia, S. Bai, J. Hartmann, D. Wang, Synthesis of monodisperse quasi-spherical gold nanoparticles in water via silver(I)-assisted citrate reduction. *Langmuir* **26**, 3585–3589 (2010). doi:[10.1021/ja902987w](https://doi.org/10.1021/ja902987w)
185. B.T. Teranishi, I. Kiyokawa, M. Miyake, Synthesis of monodisperse gold nanoparticles using linear polymers as protective agents. *Adv. Mater.* **10**, 596–599 (1998). doi:[10.1002/\(SICI\)1521-4095\(199805\)10:8<596:AID-ADMA596>3.0.CO;2-Y](https://doi.org/10.1002/(SICI)1521-4095(199805)10:8<596:AID-ADMA596>3.0.CO;2-Y)

186. J.S. Oh, L.N. Dang, S.W. Yoon, P.C. Lee, D.O. Kim, K.J. Kim, J.D. Nam, Amine-functionalized polyglycidyl methacrylate microsphere as a unified template for the synthesis of gold nanoparticles and single-crystal gold plates. *Macromol. Rapid Commun.* **34**, 504–510 (2013). doi:[10.1002/marc.201200713](https://doi.org/10.1002/marc.201200713)
187. J. Liu, P.-Y. Gu, N.-J. Li, L.-H. Wang, C.-Y. Zhang, Q.-F. Xu, J.-M. Lu, Preparation of a polymer containing indole groups by RAFT polymerization and one-phase synthesis of AuNPs-polymer nanocomposites. *J. Appl. Polym. Sci.* **129**, 2913–2921 (2013). doi:[10.1002/app.39026](https://doi.org/10.1002/app.39026)
188. J. Wagner, J.M. Köhler, Continuous synthesis of gold nanoparticles in a microreactor. *Nano Lett.* **5**, 685–691 (2005). doi:[10.1021/nl050097t](https://doi.org/10.1021/nl050097t)
189. Y.-C. Yeh, B. Creran, V.M. Rotello, Gold nanoparticles: preparation, properties, and applications in bionanotechnology. *Nanoscale* **4**, 1871–1880 (2012). doi:[10.1021/cm049532v](https://doi.org/10.1021/cm049532v)
190. H. Hiramatsu, F.E. Osterloh, A simple large-scale synthesis of nearly monodisperse gold and silver nanoparticles with adjustable sizes and with exchangeable surfactants. *Chem. Mater.* **16**, 2509–2511 (2004). doi:[10.1021/cm049532v](https://doi.org/10.1021/cm049532v)
191. L. Dykmana, N. Khlebtsov, Gold nanoparticles in biomedical applications: recent advances and perspectives. *Chem. Soc. Rev.* **41**, 2256–2282 (2012). doi:[10.1039/C1CS15166E](https://doi.org/10.1039/C1CS15166E)
192. M. Schulz-Dobrick, K.V. Sarathy, M. Jansen, Surfactant-free synthesis and functionalization of gold nanoparticles. *J. Am. Chem. Soc.* **127**, 12816–12817 (2005). doi:[10.1021/ja054734t](https://doi.org/10.1021/ja054734t)
193. S.N. Baker, G.A. Baker, Luminescent carbon nanodots: emergent nanolights. *Angew. Chem. Int. Ed.* **49**, 6726–6744 (2010). doi:[10.1002/anie.200906623](https://doi.org/10.1002/anie.200906623)
194. S.C. Ray, A. Saha, N.R. Jana, R. Sarkar, Fluorescent carbon nanoparticles: synthesis, characterization, and bioimaging application. *J. Phys. Chem. C* **113**, 18546–18551 (2009). doi:[10.1021/jp905912n](https://doi.org/10.1021/jp905912n)
195. H.T. Li, Z.H. Kang, Y. Liu, S.-T. Lee, Carbon nanodots: synthesis, properties and applications. *J. Mater. Chem.* **22**, 24230–24253 (2012). doi:[10.1039/C2JM34690G](https://doi.org/10.1039/C2JM34690G)
196. H. Wu, X. Huang, M.M. Gao, X.P. Liao, B. Shi, Polyphenol-grafted collagen fiber as reductant and stabilizer for one-step synthesis of size-controlled gold nanoparticles and their catalytic application to 4-nitrophenol reduction. *Green Chem.* **13**, 651–658 (2011). doi:[10.1039/C0GC00843E](https://doi.org/10.1039/C0GC00843E)
197. S.M. Henrichs, S.F. Sugai, Adsorption of amino acids and glucose by sediments of Resurrection Bay, Alaska, USA: functional group effects. *Geochim. Cosmochim. Acta* **57**, 823–835 (1993). doi:[10.1016/0016-7037\(93\)90171-R](https://doi.org/10.1016/0016-7037(93)90171-R)
198. L.R. Radovic, I.F. Silva, J.I. Ume, J.A. Menéndez, C.A. Leon, Y. Leon, A.W. Scaroni, An experimental and theoretical study of the adsorption of aromatics possessing electron-withdrawing and electron-donating functional groups by chemically modified activated carbons. *Carbon* **35**, 1339–1348 (1997). doi:[10.1016/S0008-6223\(97\)00072-9](https://doi.org/10.1016/S0008-6223(97)00072-9)
199. C.H. Tessmer, R.D. Vidic, L.J. Uranowski, Impact of oxygen-containing surface functional groups on activated carbon adsorption of phenols. *Environ. Sci. Technol.* **31**, 1872–1878 (1997). doi:[10.1021/es960474r](https://doi.org/10.1021/es960474r)
200. E.C. Cho, L. Au, Q. Zhang, Y.N. Xia, The effects of size, shape, and surface functional group of gold nanostructures on their adsorption and internalization by cells. *Small* **6**, 517–522 (2010). doi:[10.1002/sml.200901622](https://doi.org/10.1002/sml.200901622)
201. G. Muralidharan, L. Subramanian, S.K. Nallamuthu, V. Santhanam, S. Kumar, Effect of reagent addition rate and temperature on synthesis of gold nanoparticles in microemulsion route. *Ind. Eng. Chem. Res.* **50**, 8786–8791 (2011). doi:[10.1021/ie2002507](https://doi.org/10.1021/ie2002507)
202. T. Yang, Z. Li, L. Wang, C.L. Guo, Y.J. Sun, Synthesis, characterization, and self-assembly of protein lysozyme monolayer-stabilized gold nanoparticles. *Langmuir* **23**, 10533–10538 (2007). doi:[10.1021/la701649z](https://doi.org/10.1021/la701649z)
203. C. Jayaseelan, R. Ramkumar, A.A. Rahuman, P. Perumal, Green synthesis of gold nanoparticles using seed aqueous extract of *Abelmoschus esculentus* and its antifungal activity. *Ind. Crop. Prod.* **45**, 423–429 (2013). doi:[10.1016/j.indcrop.2012.12.019](https://doi.org/10.1016/j.indcrop.2012.12.019)

204. S.K. Das, C. Dickinson, F. Lafir, D.F. Brougham, E. Marsili, Synthesis, characterization and catalytic activity of gold nanoparticles biosynthesized with *Rhizopus oryzae* protein extract. *Green Chem.* **14**, 1322–1334 (2012). doi:[10.1039/C2GC16676C](https://doi.org/10.1039/C2GC16676C)
205. H.T. Li, X.D. He, Z.H. Kang, H. Huang, Y. Liu, J.L. Liu, S.Y. Lian, C.C.A. Tsang, X.B. Yang, S.T. Lee, Water-soluble fluorescent carbon quantum dots and catalyst design. *Angew. Chem. Int. Ed.* **49**, 4430–4434 (2010). doi:[10.1002/anie.200906154](https://doi.org/10.1002/anie.200906154)
206. D. Tang, J. Liu, X. Wu, R. Liu, X. Han, Y. Han, H. Huang, Y. Liu, Z. Kang, Carbon quantum dot/NiFe layered double-hydroxide composite as a highly efficient electrocatalyst for water oxidation. *ACS Appl. Mater. Interfaces* **6**, 7918–7925 (2014). doi:[10.1021/am501256x](https://doi.org/10.1021/am501256x)
207. L. Trotochaud, J.K. Ranney, K.N. Williams, S.W. Boettcher, Solution-cast metal oxide thin film electrocatalysts for oxygen evolution. *J. Am. Chem. Soc.* **134**, 17253–17261 (2012). doi:[10.1021/ja307507a](https://doi.org/10.1021/ja307507a)
208. Y. Lee, J. Suntivich, K.J. May, E.E. Perry, Y. Shao-Horn, Synthesis and activities of rutile IrO₂ and RuO₂ nanoparticles for oxygen evolution in acid and alkaline solutions. *J. Phys. Chem. Lett.* **3**, 399–404 (2012). doi:[10.1021/jz2016507](https://doi.org/10.1021/jz2016507)
209. M. Fekete, R.K. Hocking, S.L.Y. Chang, C. Italiano, A.F. Patti, F. Arena, L. Spiccia, Highly active screen-printed electrocatalysts for water oxidation based on β -manganese oxide. *Energy Environ. Sci.* **6**, 2222–2232 (2013). doi:[10.1039/C3EE40429C](https://doi.org/10.1039/C3EE40429C)
210. G. Abellán, E. Coronado, C. Martí-Gastaldo, E. Pinilla-Cienfuegos, A. Ribera, Hexagonal nanosheets from the exfoliation of Ni²⁺-Fe³⁺ LDHs: a route towards layered multifunctional materials. *J. Mater. Chem.* **20**, 7451–7455 (2010). doi:[10.1039/C0JM01447H](https://doi.org/10.1039/C0JM01447H)
211. D.G. Evans, X. Duan, Preparation of layered double hydroxides and their applications as additives in polymers, as precursors to magnetic materials and in biology and medicine. *Chem. Commun.* 485–496 (2006). doi:[10.1039/B510313B](https://doi.org/10.1039/B510313B)
212. G.A. Caravaggio, C. Detellier, Z. Wronski, Synthesis, stability and electrochemical properties of NiAl and NiV layered double hydroxides. *J. Mater. Chem.* **11**, 912–921 (2001). doi:[10.1039/B004542J](https://doi.org/10.1039/B004542J)
213. G. Abellán, F. Busolo, E. Coronado, C. Martí-Gastaldo, A. Ribera, Hybrid magnetic multilayers by intercalation of Cu(II) phthalocyanine in LDH hosts. *J. Phys. Chem. C* **116**, 15756–15764 (2012). doi:[10.1021/jp303537v](https://doi.org/10.1021/jp303537v)
214. O.C. Compton, S.T. Nguyen, Graphene oxide, highly reduced graphene oxide, and graphene: versatile building blocks for carbon-based materials. *Small* **6**, 711–723 (2010). doi:[10.1002/smll.200901934](https://doi.org/10.1002/smll.200901934)
215. Y. Zhang, N. Zhang, Z.-R. Tang, Y.-J. Xu, Graphene transforms wide band gap ZnS to a visible light photocatalyst. The new role of graphene as a macromolecular photosensitizer. *ACS Nano* **6**, 9777–9789 (2012). doi:[10.1021/nm304154s](https://doi.org/10.1021/nm304154s)
216. X. Huang, Z. Yin, S. Wu, X. Qi, Q. He, Q. Zhang, Q. Yan, F. Boey, H. Zhang, Graphene-based materials: synthesis, characterization, properties, and applications. *Small* **7**, 1876–1902 (2011). doi:[10.1002/smll.201002009](https://doi.org/10.1002/smll.201002009)
217. D. Tang, H. Zhang, H. Huang, R. Liu, Y. Han, Y. Liu, C. Tong, Z. Kang, Carbon quantum dots enhance the photocatalytic performance of BiVO₄ with different exposed facets. *Dalton Trans.* **42**, 6285–6289 (2013). doi:[10.1039/c3dt50567g](https://doi.org/10.1039/c3dt50567g)
218. H. Li, R. Liu, Y. Liu, H. Huang, H. Yu, H. Ming, S. Lian, S.-T. Lee, Z. Kang, Carbon quantum dots/Cu₂O composites with protruding nanostructures and their highly efficient (near) infrared photocatalytic behavior. *J. Mater. Chem.* **22**, 17470–17475 (2012). doi:[10.1039/C2JM32827E](https://doi.org/10.1039/C2JM32827E)
219. Y.M. Yang, J. Liu, Y.Z. Han, H. Huang, N.Y. Liu, Y. Liu, Z.H. Kang, Porous cobalt, nitrogen-codoped carbon nanostructures from carbon quantum dots and VB12 and their catalytic properties for oxygen reduction. *Phys. Chem. Chem. Phys.* **16**, 25350–25357 (2014). doi:[10.1039/C4CP04119D](https://doi.org/10.1039/C4CP04119D)
220. N. Alexeyeva, K. Tammeveski, Electroreduction of oxygen on gold nanoparticle/PDDA-MWCNT nanocomposites in acid solution. *Anal. Chim. Acta* **618**, 140–146 (2008). doi:[10.1016/j.aca.2008.04.056](https://doi.org/10.1016/j.aca.2008.04.056)

221. Z. Jin, H. Nie, Z. Yang, J. Zhang, Z. Liu, X. Xu, S. Huang, Metal-free selenium doped carbon nanotube/graphene networks as a synergistically improved cathode catalyst for oxygen reduction reaction. *Nanoscale* **4**, 6455–6460 (2012). doi:[10.1039/C2NR31858J](https://doi.org/10.1039/C2NR31858J)
222. X. Ma, H. Meng, M. Cai, P.K. Shen, Bimetallic carbide nanocomposite enhanced Pt catalyst with high activity and stability for the oxygen reduction reaction. *J. Am. Chem. Soc.* **134**, 1954–1957 (2012). doi:[10.1021/ja2093053](https://doi.org/10.1021/ja2093053)
223. X. Xia, F. Zhang, X. Zhang, P. Liang, X. Huang, B.E. Logan, Use of pyrolyzed iron ethylenediaminetetraacetic acid modified activated carbon as air-cathode catalyst in microbial fuel cells. *ACS Appl. Mater. Interfaces* **5**, 7862–7866 (2013). doi:[10.1021/am4018225](https://doi.org/10.1021/am4018225)
224. Z.-S. Wu, L. Chen, J. Liu, K. Parvez, H. Liang, J. Shu, H. Sachdev, R. Graf, X. Feng, K. Müllen, High-performance electrocatalysts for oxygen reduction derived from cobalt porphyrin-based conjugated mesoporous polymers. *Adv. Mater.* **26**, 1450 (2014). doi:[10.1002/adma.201304147](https://doi.org/10.1002/adma.201304147)
225. B. Piela, T.S. Olson, P. Atanassov, P. Zelenay, Highly methanol-tolerant non-precious metal cathode catalysts for direct methanol fuel cell. *Electrochim. Acta* **55**, 7615–7621 (2010). doi:[10.1016/j.electacta.2009.11.085](https://doi.org/10.1016/j.electacta.2009.11.085)
226. S.-T. Chang, H.-C. Huang, H.-C. Wang, H.-C. Hsu, J.-F. Lee, C.-H. Wang, Effects of structures of pyrolyzed corrin, corrole and porphyrin on oxygen reduction reaction. *Int. J. Hydrogen Energy* **39**, 934–941 (2014). doi:[10.1016/j.ijhydene.2013.10.082](https://doi.org/10.1016/j.ijhydene.2013.10.082)
227. J.H. Zagal, M. Páez, C. Páez, Reactivity of immobilized cobalt phthalocyanines for the electroreduction of molecular oxygen in terms of molecular hardness. *J. Electroanal. Chem.* **489**(1), 96–100 (2000). doi:[10.1016/S0022-0728\(00\)00209-6](https://doi.org/10.1016/S0022-0728(00)00209-6)
228. H.-W. Liang, W. Wei, Z.-S. Wu, X.L. Feng, K. Müllen, Mesoporous metal–nitrogen-doped carbon electrocatalysts for highly efficient oxygen reduction reaction. *J. Am. Chem. Soc.* **135**, 16002–16005 (2013). doi:[10.1021/ja407552k](https://doi.org/10.1021/ja407552k)
229. S.-T. Chang, C.-H. Wang, H.-Y. Du, H.-C. Hsu, C.-M. Kang, C.-C. Chen, J.C.S. Wu, S.-C. Yen, W.-F. Huang, L.-C. Chen, M.C. Linf, K.-H. Chen, Vitalizing fuel cells with vitamins: pyrolyzed vitamin B₁₂ as a non-precious catalyst for enhanced oxygen reduction reaction of polymer electrolyte fuel cells. *Energy Environ. Sci.* **5**, 5305–5314 (2012). doi:[10.1039/C1EE01962G](https://doi.org/10.1039/C1EE01962G)